Burov E., Part 1 Surficial and Deep Porcesses in Thrust Belts, Chapter 1: Coupled lithosphere-surface processes in collision context, Eds: O. Lacombe, J. Lavé, F. Roure and J. Vergès, "Thrust belts and foreland basins: From fold kinematics to hydrocarbon systems", series " Frontiers in Earth Sciences", Springer-Verlag, Berlin Heidelberg, p 1-40, ISBN-13: 978-3-540-69425-0, 2007

Coupled Lithosphere-Surface Processes in Collision Context

Evgueni Burov

Abstract. From the mechanical point of view, a mountain range that exceeds a certain critical height (of about 3 km in altitude, depending on rheology and width) should flatten and collapse within few My as a result of gravitational spreading of its ductile crustal root. Even if the crustal root does not collapse, the mountain range would be levelled by gravity sliding and other surface processes that, in case of static topography, lead to its exponential decay with a characteristic time constant on the order of 2.5 My. However, in nature, mountains grow and stay as localized tectonic features over geologically important periods of time (> 10 My). To explain the paradox of long-term persistence and localized growth of the mountain belts, a number of workers have emphasized the importance of dynamic feedbacks between surface processes and tectonic evolution. Indeed, surface processes modify the topography and redistribute tectonically significant volumes of sedimentary material, which acts as vertical loading over large horizontal distances. This results in dynamic loading and unloading of the underlying crust and mantle lithosphere, whereas topographic contrasts are required to set up erosion and sedimentation processes. Tectonics therefore could be a forcing factor of surface processes and vice versa. One can suggest that the feedbacks between tectonic and surface processes are realized via two interdependent mechanisms:

1. Slope, curvature and height dependence of the erosion/deposition rates
2. Surface load-dependent subsurface processes such as isostatic rebound and lateral ductile flow in the lower or intermediate crustal channel.

Loading/unloading of the surface due to surface processes results in lateral pressure gradients, that, together with low viscosity of the ductile crust, may permit rapid relocation of the matter both in horizontal and vertical direction (upward/downward flow in the ductile crust). In this paper, we overview a number of coupled models of surface and tectonic processes, with a particular focus on 3 representative cases:

1. Slow convergence and erosion rates (Western Alpes)
2. Intermediate rates (Tien Shan, Central Asia)
3. Fast convergence and erosion rates rates (Himalaya, Central Asia).

1 Introduction

Continental mountain belts, such as, for example, Tien Shan (Central Asia, Figure 1a), are characterized by highly localized topography elevations persistently growing over tens of millions of years. The fact that gravitational potential energy per unit surface $0.5\rho gh^2$ scales as h^2 implies that a thrust belt should grow more easily in width than in height (Molnar and Lyon-Caen, 1988, h is the mean topography elevation above sea level, ρ is density and g is acceleration due to gravity). A portion of continental crust submitted to quasi-static horizontal shortening should tend to thicken homogeneously. This can be put another way around by considering that a range results from thrusting on faults that cut through the upper crust and root into the lower crust. Uplift of the range implies an increase in the vertical stress acting on the fault. This acts to oppose further frictional sliding on the fault, inhibiting further thrusting. A new fault will then form farther away from the range front leading to widening of the range. In addition, erosion and sedimentation at the surface, together with flow in the lower crust, should favor smoothing of topographic irregularities. At the pressure and temperature conditions of the lower crust, most crustal rocks are thought to flow easily at very low deviatoric stresses (e.g., Brace and Kohlstedt, 1980; Wang et al., 1994, Fig. 2a). The deviatoric stresses associated with slopes of the topography and of the Moho (e.g., Fleitout and Froidevaux, 1982) should therefore be relaxed by viscoplastic flow in the ductile lower crust inducing decay of topographic irregularities (Kusznir and Matthews, 1988; Gratton, 1989; Bird, 1991, Fig. 1b).

The growth and maintenance of topographic features at the surface of continents might be taken to indicate that the strength of the crust exceeds the deviatoric stresses associated with slopes of the topography and of the Moho. Yet, as mentioned above, laboratory experiments indicate that at the pressure and temperature conditions of the lower crust, most crustal rocks should flow easily. Irregularities of the topography and of the Moho boundary should therefore be

Burov E., Part 1 Surficial and Deep Porcesses in Thrust Belts, Chapter 1: Coupled lithosphere-surface processes in collision context, Eds: O. Lacombe, J. Lavé, F. Roure and J. Vergès, "Thrust belts and foreland basins: From fold kinematics to hydrocarbon systems", series " Frontiers in Earth Sciences", Springer-Verlag, Berlin Heidelberg, p 1-40, ISBN-13: 978-3-540-69425-0, 2007

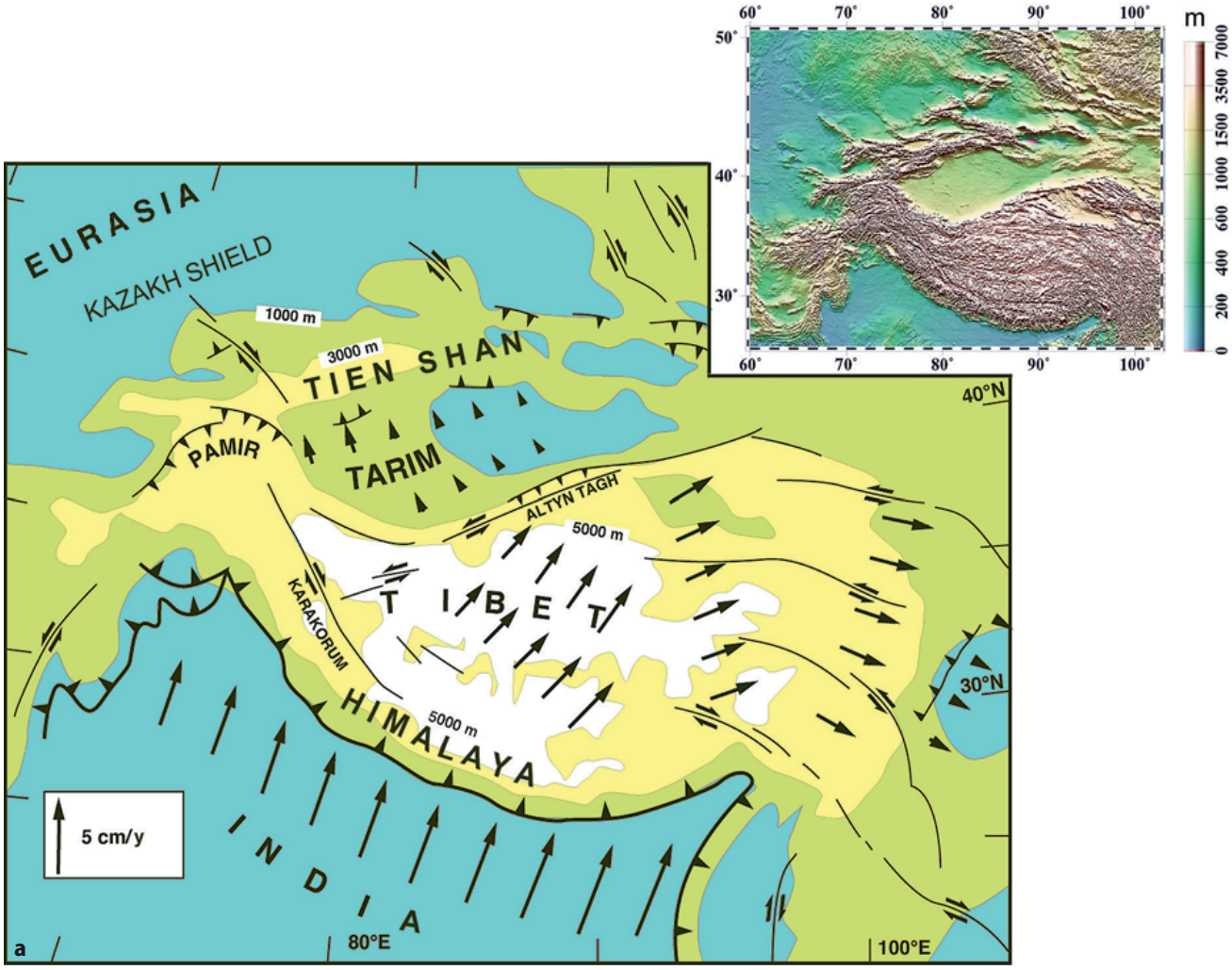

Fig. 1a. Actively growing intercontinental belts and plateaux: an example showing a schematic map of India-Eurasia collision with its main features such as the Himalayan mountain belt, Tibetan plateau, Tarim basin, Pamir and Tien Shan mountain belt. Insert shows a digital elevation map of the same area. The topography peaks to 8800 m in the Himalayas (Everest) and 7500 m in Tien Shan (Pobeda Peak). Modified after (Avouac and Tapponier, 1993)

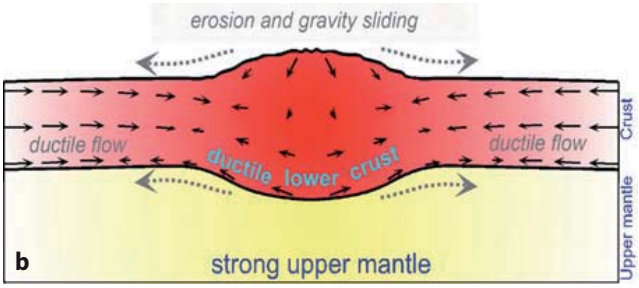

Fig. 1b. Erosional and gravity collapse of a mountain range (e.g., Gratton, 1989; Bird, 1991). In the conceptual model shown here, there is no balance between surface and subsurface processes. Even if such range was created somehow, it will not persist, as its root and topography will be flattened in about 2 My in the absence of some compensating mechanisms. Tectonic convergence may not solely compensate this flattening; it may only grant an overall thickening of the crust; some additional localizing mechanisms are needed to concentrate thickening in a narrow range.

relaxed by viscoplastic flow in the ductile lower crust and decay with time (Kusznir and Matthews, 1988; Gratton, 1989; Bird, 1991). Consider, for example, the Tien Shan range, which is, except for the Himalayas, the largest and most active intracontinental range in the world (Fig. 1a). Tien Shan (translated as "Heavenly Mountains") is 300–400 km wide in its central area, with a mean elevation of about 3500 m and local peaks of up to 7500 m, in a zone of relatively thick and tectonized crust (Moho depths from 50 to 70 km) (e.g., Avouac et al., 1993). The Tien Shan is a continuously growing range, that has started to rise 10–15 My ago. A simple dimensional analysis (Gratton, 1989) as well as numerical simulations (Bird, 1991; Avouac and Burov, 1996; Burov and Watts, 2006) show that the topography of such a range should, instead of growing, be reduced by half in a few My (Fig. 1b). This estimate is based on the assumption of ductile rheology of the

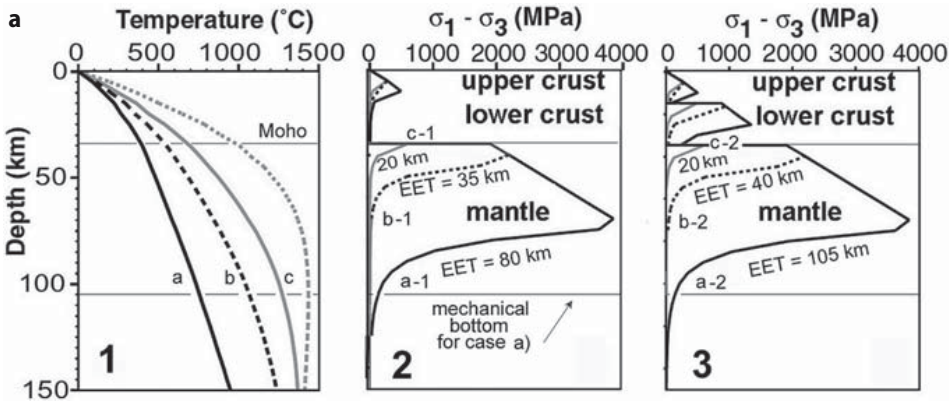

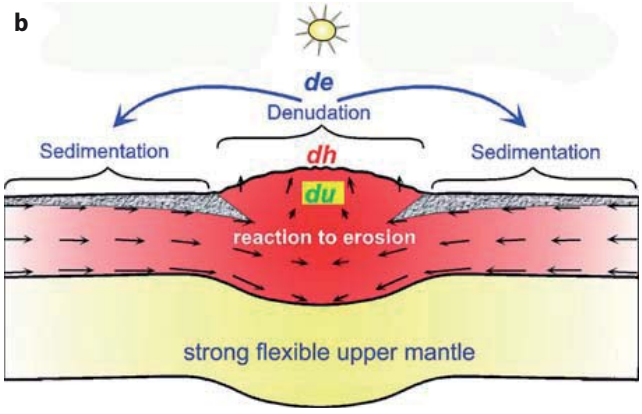

Fig. 2. **a**) Typical rheology profiles for continental lithosphere indicate the possibility for lower-crustal flow: (*1*) geotherms that yield YSEs shown in the middle and on the right; (*2*) yield stress envelope (YSE) for quartz-rich upper and lower crust and olivine mantle; (*3*) yield stress envelope (YSE) for quartz-rich upper crust , diabase lower crust, olivine mantle. EET – equivalent elastic thickness of the lithosphere computed for each of YSEs. **b**) Solution to the problem stated in Fig. 1b: a conceptual model of continental collision in which strong feedback between surface processes, isostatic reaction and subsurface crustal flow results in accelerated growth of topography in the area of strongest subsurface uplift

lower crust, which is supported for this area by multiple data starting from seismic data (Vinnik and Saipbekova, 1984; Makeyeva, 1992; Roecker et al., 1993; Vinnik et al., 2006) and ending by gravity-flexural analysis (Burov et al., 1990, 1993; Avouac and Burov, 1996). Only the short topographic wavelengths, typically less than a few tens of kilometers that can be supported by the strength of the upper crust would be maintained over geological periods of time, yet provided that they are not wiped out by erosion, which is faster on short wavelength features. In addition, surface processes might be thought to contribute to an even more rapid smoothing of the topography. Similarly, in the absence of strong rheological heterogeneities or of strain localization processes, a portion of a continental crust submitted to horizontal shortening should tend to thicken homogeneously, so that no mountain should form. The growth and maintenance of an intracontinental mountain range over long periods of time must therefore involve dynamical processes allowing for long-term localization of lithospheric strain below the mountain.

Several mechanisms have been advocated to explain localization of major thrust faults and, by its proxy, stability of mountain belts. Intrinsic strain softening properties of rocks could sustain localized thrust faulting at the crustal scale. Alternatively, a range could result from shear stresses at base of the crust induced by lithospheric under-thrusting or by mantle dynamics (e.g., Beaumont et al., 1994; Ellis et al., 1995). Such a mechanism may be suggested for mountains associated with subduction zones or with hotspots (Vogt, 1991), but seems inappropriate to explain most intracontinental mountains. In the case of, for example, the Tien Shan belt, a particular mantle dynamics has been inferred from gravity modelling (Burov et al., 1990, 1993) and seismic anisotropy (Makeyeva, 1992; Roecker et al., 1993), but we contend that it might not be the key factor. Our point is instead that coupling between surface processes and flow in the lower crust could provide an alternative and more general explanation (Avouac and Burov, 1996; Burov and Cloetingh, 1997).

To explain the paradox of long-term mountain persistence and localized growth, a number of workers have emphasized the importance of dynamic feedbacks between surface processes and tectonic evolution (e.g., Molnar and England, 1990; Masek et al., 1994a; Avouac and Burov, 1996; Molnar, 2001). Indeed, surface processes modify the topography and redistribute tectonically significant volumes of sedimentary material (vertical, or normal loads) over large horizontal distances. This may result in dynamic loading and unloading of the underlying crust and mantle lithosphere, whereas topographic contrasts are required to set up erosion and sedimentation processes.

Tectonics therefore could be a forcing factor of surface processes.

In this paper, we first review the existing models of surface processes and the thermo-mechanical properties of the lithosphere that condition its response to surface and tectonic loading-unloading. We then review our own and other previous modelling studies that show that surface and tectonic processes are not independent processes and can interact. We show in particular that advection of material at the Earth's surface and horizontal flow in the crust might be coupled so as to permit mountain growth in response to horizontal shortening. This mechanism is then validated and investigated on the basis of semi-analytical and numerical experiments in which the rheological layering of the lithosphere and surface processes are modelled. We then find that, depending of the erosion rate compared to horizontal shortening, flow in the lower crust can be "outward" (from under the high topography) or "inward" (toward the crustal root of a high topography). When inward flow occurs, a mountain range can actually grow and no other mechanism is required to explain localized uplift. Some implications about the role of climate on continental tectonics and on the geomorphology of mountain ranges are then derived.

We suggest an additional feedback mechanism by lateral crustal flow (Fig. 2b). According to this mechanism, erosional removal of material from topographic heights (dynamic unloading) and its deposition in the foreland basins (dynamic loading) should result in horizontal ductile crustal flow that may oppose gravitational spreading of the crustal roots and may eventually drive a net influx of material towards the orogeny. We finally test our ideas on three representative and well-studied cases:

1. Slow convergence and erosion rates (Western Alpes),
2. Intermediate rates (Tien Shan, Central Asia), and
3. Fast convergence and erosion rates rates (Himalaya, Central Asia).

2 Interplays Between Surface and Tectonic Processes

2.1 Tectonic Forcing on Surface Processes

Surface topography elevations are required to set up erosion and sedimentation processes. Tectonics is therefore a forcing factor of surface processes. Following Ahnert (1970), and Pinet and Souriau (1988), Summerfield and Hulton (1994) have compiled rates of denudation at the scale of major river basins. These studies indicate that denudation is primarily influenced by basin topography so that rates of denudation appear to be systematically high in areas of active tectonic uplift. Common values of mean denudation rates in such areas would be of the order of a few 0.1 mm/y to about 1mm/y at the scale of large drainage basins. Such rates are generally consistent with estimates derived from balancing sediment volumes over geological periods of time (Leeder, 1991; Summerfield and Hulton, 1994). Thermochronologic studies indicate, however, local values as great as 1 mm/y (see Leeder, 1991 and Molnar and England, 1990, for critical reviews). The discrepancy between local and basin averaged estimates is due to the fact that tectonic uplift is probably distributed in brief pulses over localized domains within a drainage basin (Copeland and Harrison, 1990). In the absence of any tectonic feedback, common values of denudation rates should lead to the disappearance of a major mountain belt like the Alpes or Tien Shan in a few million years. Pinet and Souriau (1988) demonstrated that denudation leads to an exponential decay of the topography of a range with a characteristic time constant of the order of 2.5 m.y.

2.2 Coupling Between Denudation and Tectonic Uplift due to Isostasy

Many recent models have investigated coupling between the isostatic reaction and surface processes (e.g., Kooi and Beaumont, 1994; Snyder et al., 2000; Basile and Allemand, 2002; Garcia-Castellanos, 2002; Garcia-Castellanos et al., 2002; 2003; Simpson and Schlunegger, 2003; Persson et al., 2004; Casteltort and Simpson, 2006). Redistribution of surface loads by erosion and sedimentation must induce tectonic deformation to maintain isostatic balance. Vertical uplift is expected to partly compensate unloading in the area subjected to denudation while subsidence should occur in response to loading by sedimentation. This feedback mechanism may lead to some coupling between denudation and tectonic uplift (e.g., Ahnert, 1970). A first consequence is that the time needed to erode a topographic relief must take into account removal of the topographic relief and of the crustal root. If local isostasy is assumed and if horizontal strains are neglected, denudation is dynamically compensated by uplift and the characteristic time of decay of the topography would then be of the order of 10 m.y. (Leeder, 1991). In addition, it has been argued that a positive feedback may arise (Molnar and England, 1990; Masek et al., 1994b). If the slopes of valleys steepen during river incision, isostatic readjustment following denudation in a mountain range may result in a net uplift of the higher summits in spite of the average lowering of reliefs. Alternatively regional compensation due to the elasticity of the lithosphere might lead to the uplift of the

eroded edge of a plateau. Erosion might therefore induce some uplift of topographic summits leading in turn to enhanced erosion. The uplift of the Himalayan belt during the last few million years may have resulted from such a coupling rather than from thrusting at the Himalayan front (Burbank, 1992; Burbank and Verges, 1994). Note however that, while the peaks might reach higher elevations following isostatic adjustment, the net effect of erosion is crustal thinning. Thus, these models cannot explain the growth of mountains over long time periods.

The strongest feedback between erosion and isostatic reaction would be obtained for local isostasy. It will be mitigated in case of more regional compensation and become negligible for lithospheres whose equivalent elastic thickness exceeds 60 km. This is another reason to support the idea that more efficient mechanisms should also take place in collisional settings.

2.3 Coupling Between Surface Processes and Horizontal Strains

As mentioned in the introduction, small lateral variations of the crustal thickness should drive horizontal flow in the lower crust. Some studies have already pointed out to the importance of such a process in continental tectonics (e.g., Lobkovsky, 1988; Lobkovsky and Kerchman, 1991; Burov and Cloetingh, 1997). For example, Kruse et al. (1991) have shown that horizontal flow in the lower crust has regulated isostatic equilibrium during extension in the Basin and Range. The lower crust would have been extruded from under the high topography during that process. Following Westaway (1994) we will call this sense of flow "outward". On the other hand, Gregory and Chase (1994) inferred "inward" flow, toward the crustal root, during the Laramide orogeny of the Frontal Range, Colorado. The characteristic time associated with flow in the lower crust induced by the topography of a range a few thousands of meters high, a few hundreds of km wide, is in the order of a few m.y. The characteristic times of erosional decay of the topography of a range and of lateral collapse of a crustal root are thus of the same order of magnitude. Since both processes are driven by topographic slopes, some coupling may arise. Although it is not often pointed out, it has long been recognized that this kind of process might play a major role in elevation changes within continents (see Westaway, 1994 for an review of historical development of these ideas). Westaway (1994) made a case for such a coupling, with inward flow, in the context of extensional tectonics in western Turkey. He proposed that sediment loading in the sedimentary basins would have driven flow toward the uplifted area. This kind of process was first modelled by King and Ellis (1990), who modelled crustal extension using a thin elastic plate (upper crust) overlying an inviscid fluid (lower crust).

We propose that this kind of coupling might also appear in a compressional context. Let us consider a portion of a lithosphere, loaded with some initial range topography in regional isostatic balance, and submitted to horizontal compression. Horizontal stress gradients, resulting from the slopes of the topography and of the Moho, must drive horizontal flow. The lithosphere in the region of the range is weakened, since the crust is thick and hot, and because bending of the lithosphere beneath the mountain load tends to reduce its strength (Burov and Diament, 1992; 1995; Ranalli, 1995). Higher strain rates in the area below the range should therefore be expected. A low viscosity channel in the lower crust beneath the high topography might therefore allow lateral flow. In the absence of horizontal shortening and erosion, the lower crust below the range would be extruded laterally as discussed by Bird (1991). If erosion takes place, a regime may be established in which horizontal shortening would be preferentially accommodated by crustal thickening in the area below the range:

a) Surface processes remove material from the range and feed the adjacent flexural basins inducing isostatic imbalance.
b) This imbalance produces a temporary excess of normal stress below the foreland basins and deficit below the range favoring flow in the lower crust towards the crustal root. The range uplifts and the basins subside.

Ultimately this coupled regime might lead to some dynamic equilibrium in which the amount of material removed by erosion would balance the material supplied to the range by subsurface deformation.

Apart of the direct mechanical effect of erosion/sedimentation (loading-unloading) on the lithosphere, it also has very important thermal, and, by proxy, mechanical consequences, because the removal and accumulation of sedimentary matter modifies surface heat flux and thermal conditions in the upper crust (e.g., England and Richardson, 1977). Accumulation of sediments in the forelands leads to (1) cooling of the accretion wedge at a short term, in case of rapid advection/filling (initial stages of collision when the convergence rate is highest); (2) heating of the accretion wedge at a long term in case of slow advection (when collision rate slows down), due to heat screening (sediments have low thermal conductivity) and the abundance of heat producing radiogenic elements in the sedimentary matter. Furthermore, penetration of the mechanically weak sediment in the subduction channel should serve as lubrification and may enhance the conditions for subduction processes.

2.4 Coupling of Surface Processes and Tectonic Input/Reaction in Full Scale Mechanical Models: Major Stages

A number of earlier modelling studies (e.g., Beaumont, 1981; Beaumont et al., 1992; 1995; Willet, 1999) have investigated various relationships between erosion and tectonic processes. However, tectonic reaction was not fully accounted for, as most of these models that have exploited semi-kinematic formulations for the crust or the mantle lithosphere. One of the first full-scale parametric semi-analytical models was developed by Avouac and Burov (1996) in order to validate the coupled regime between surface and subsurface processes. For this purpose this model accounted for:

1. Surface processes.
2. The effect of topographic loads and variations of crustal thickness on the mechanical behavior of the lithosphere.
3. Ductile flow in the lower crust.
4. Depth-and-strain dependent rheology of the lithosphere.

In the following sections we first discuss the components needed to build a coupled tectonic model of orogenic building:

1. The existing models of surface processes.
2. The rheology data needed for proper account of the mechanical response of the lithosphere.
3. Thermal models of the lithosphere needed for proper account of thermally dependent ductile rheology.

We then describe the design and major results of the coupled semi-analytical model of Avouac and Burov (1996). This semi-analytical model has a number of limitations in terms of model geometry and its inability to account for some key deformation modes such as formation of major thrust faults. For this reason, in the final sections of this study, we go further by introducing an unconstrained fully coupled numerical thermo-mechanical model of continental collision/subduction similar to that used by Burov et al., (2001); and Toussaint et al. (2004a,b). This model takes into account more realistic (than in the previous studies) geometry of the convergent plates, accounts for large strains and brittle-elastic-ductile rheology including localized brittle (faulting) and ductile deformation.

3 Surface Processes Modelling: Principles and Numerical Implementation

3.1 Basic Models of Surface Processes

A growing amount of field and experimental studies have investigated and validated various forms of long-and-short range erosion and sedimentary transport laws and models (Ahnert, 1970; Beaumont, 1981; Beaumont et al., 1992;2000; Burbank, 1992; Burbank and Verge, 1994; Ashmore, 1982; Mizutani, 1998; Lavé and Avouac, 2001; Lague et al., 2000, 2003; Davy and Grave, 2000; Lague et al, 2000; Molnar, 2001; Grave and Davy, 2001; Densmore et al., 1997;1998; Pinet and Souriau, 1988).

Short-range erosion. A simple two-dimensional law may be used to simulate erosion and sedimentation at the scale of a mountain range. The evolution of a landscape results from the combination of weathering processes that prepare solid rock for erosion, and transportation by hillslope and stream processes (see Carson and Kirkby, 1972 for a review). Although many factors, depending on the lithologies and on climate (e.g., Fournier, 1960; Nash, 1980), may control this evolution, quite simple mathematical models describing the geometrical evolution of the morphology at the small scale have been proposed and tested successfully (e.g., Kirkby, 1971; Smith and Bretherton, 1972; Chorley et al., 1984; 1986; Luke, 1972; 1974; Kirkby et al., 1993). For example, the two-dimensional evolution of a scarp-like landform can be modelled assuming that the rate of downslope transport of debris, q, is proportional to the local slope, ∇h (Culling, 1960; 1965; Hanks et al., 1984; Avouac, 1993; Kooi and Beaumont, 1994; 1996; Braun and Sambridge, 1997).

$$q = -k\nabla h \tag{1}$$

where k is the mass diffusivity coefficient, expressed in units of area per time [e.g., m^2/y]. Assuming conservation of matter along a 2-D section and no tectonic deformation, h must obey:

$$dh/dt = -\nabla q \tag{2}$$

With constant k, Eqs. (1) and (2) lead to the linear diffusion equation:

$$dh/dt = k\nabla^2 h \tag{3}$$

This model of surface processes holds only for particular conditions. The regolith must form more rapidly than it is removed by surface transport and slopes

must not exceed the frictional angle of the material. Even for scarps formed in loose alluvium some complications arise when high scarps are considered. Scarps with height typically in excess of about 10 meters in arid climatic zones, tend to have systematically sharper curvatures at crest than at base (e.g., Andrews and Bucknam, 1987). Gravity-driven erosion processes such as hillslope landsliding impose strong limitations on the applicability of the diffusion equation since the processes are rather slope- then curvature-dependent, which basically requires to introduce slope-and-height dependent terms in the equation (3). At the larger scale, hillslope and stream processes interact and the sediment transport then depends nonlinearly on the slope and on other factors such as the slope gradient, the area drained above the point, the distance from the water divide, so that the simple 2-D linear diffusion does not apply in general (e.g., Gossman, 1976). In spite of these limitations, we have chosen to stick to a linear diffusion law to model erosion in the upland. This model does not accurately mimic the spatial distribution of denudation in the mountain range but it leads to a sediment yield at the mountain front that is roughly proportional to the mean elevation of the basin relative to that point (a rough approximation to the sediment yield resulting from a change of elevation h over a horizontal distance d is $k \times h/d$) and therefore accounts for the apparent correlation between elevation and denudation rates (Ahnert; 1970, Pinet and Souriau, 1988; Summerfield and Hulton, 1994). We did not apply the diffusion model to the whole system, however. We felt that we should take into account the major discontinuity in surface processes that occurs at the mountain front. As a river emerges into the adjacent basin its gradient is sharply reduced and deposition occurs. The streams shift from side to side and build up alluvial fans and tend to form a broad gently sloping pediment at the base of the mountain range. In addition, a lateral drainage often develops along the foothills of mountain ranges. The Ganges along the Himalayan foothills, the Parana along the Andes, or the Tarim along the Tien Shan are good examples. Altogether the formation of the pediment and lateral drainage tend to maintain gentle slopes in the foreland. There is therefore a sharp contrast between river incision that maintains a rugged topography with steep slopes in the mountain range and widespread deposition of alluvium in the foreland. This discontinuity of processes must be considered to model the sharp break-in-slope at the mountain front that is generally observed on topographic profiles across mountain belts. In order to simulate this major change in surface processes, sedimentation in the lowland is modelled assuming flat deposition by fluvial network: we assume that conservation of matter along the section and the sediment at the mountain front is distributed in order to maintain a flat horizontal topography in the foreland. We arbitrarily set the change from diffusional erosion to sedimentation ("flat deposition") at a differential elevation of 500 m, which is, however, representative for the transition from highlands to forelands.

We considered values for k varying between 10^2 to 10^4 m^2/y that yield denudation rates of the order of a few 0.01 mm/y to 1 mm/y for a 200–400 km-wide range with a few thousand meters of relief. In order to test the sensitivity of our model on the assumed erosion law we also considered non linear erosion laws of the form:

$$dh/dt = k^*(x,h,\nabla h)\nabla^2 h \qquad (4a)$$

where $k^*(x,h,\nabla h) = k(x)(\nabla h)^n$ (e.g., Gossman, 1976; Andrews and Bucknam, 1987). We will refer to the cases with n = 1, 2 as first-and second-order diffusion, respectively. In these cases we did not introduce the change in regime at the mountain front since the nonlinear effects already tend to form relatively smooth pediments. It should be noted that Eq. (4) differs from the one obtained assuming a non linear diffusion coefficient in Eq. (1). In that case conservation of mass would lead to an additional term $\nabla k^* \nabla h$:

$$dh/dt = k^*(x,h,\nabla h)\,\nabla^2 h + \nabla k^*(x,h,\nabla h)\nabla h \qquad (4b)$$

However, Eq. 4a is a phemenological one and may reflect the possibility of material loss from the system. It is also noteworthy that the existing nonlinear erosion laws are not limited to Eq. 4a (e.g., Newman, 1983; Newman et al., 1990), which only presents the simplest way to account for dependence of erodibility on the morphology.

Long-range surface processes. The long-range surface processes are associated with fluvial transport, i.e., with river incision, slope geometry, character of sediment matter, and conditions for deposition (Flint, 1973; 1974; Sheperd and Schumm, 1974; Hirano, 1975; Schumm et al., 1987; Seidl and Dietrich, 1992; Govers 1992a,b; Hairsine and Rose, 1992; Sklar and Dietrich, 1998;2001; Howard et al., 1994; Howard, 1998; Smith, 1998; Davy and Crave, 2000; Snyder et al., 2000; Snyder, 2001; Hancock and Willgoose, 2001; Simpson, 2004). The characteristic laws for this range are different as these mechanisms are dependent on the incision and transport capacity of the fluvial network, local slope, and type of sediment. Deep steep rivers can carry sediment longer distances as it can be caught in turbulent flow layer. Shallow rivers would deposit sediment rapidly resulting in rapid river blockage and frequent change of the direction of the fluvial network. There is also a strong dependence of transport capaci-

ty on the grain size and climate episodicity (e.g., Davy and Crave, 2000). The long-range fluvial models were used with success by Kooi and Beamount (1994; 1996), Garcia-Castellanos (2002), Garcia-Castellanos et al. (2002; 2003), Persson et al. (2004). The cumulative material flow, q_{fe}, due to the fluvial transport can be presented, in most simple form, as:

$$q_{\mathrm{fe}} = -K_r\, q_r\, dh/dl \tag{4c}$$

where q_r is the river discharge, K_r is nondimensional transport coefficient and dh/dl is the slope in the direction of the river drainage with l being the distance along the transporting channel. The diffusion equation (4a), except if it is not strongly nonlinear, provides symmetrical, basically over-smoothed shapes whereas the fluvial transport equation (4c) may result in realistic asymmetric behaviors, because, locally, the direction of each bifurcation of the fluvial network is affected by negligibly small factors, even though the overall direction of the flow is controlled by the regional slope of topography (Fig. 3). Any important change in the regional slope of topography, such as at the transition from tectonically built steep highlands to flat sedimentary built forelands, may result, at some moment, in a drastic change of the direction of the fluvial network, which may choose a principally new stream direction orthogonal to the highland network (as it is the case for the Ganges river, for example). This happens when the sedimentary basin is filled to a point that the inclination of its surface in the direction of tectonic convergence becomes less important than that in some other direction (basically in the direction of the boundary between the steep highlands and flat lowlands).

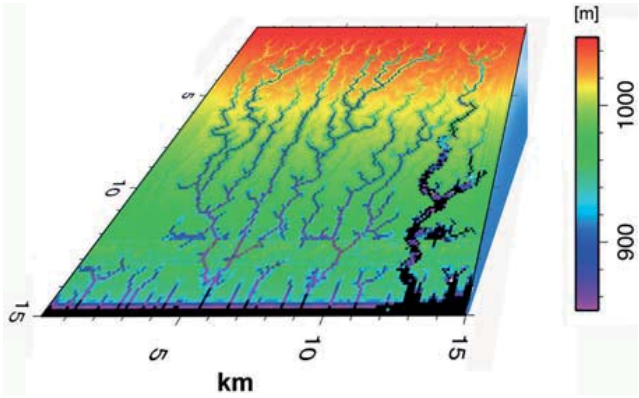

Fig. 3. Example of a typical numerical morphology model with surface erosion and sedimentation based on linear diffusion erosion equation and fluvial transport equation (Poisson, et al., 1996). Diffusion equation, except if it is not strongly non-linear, provides symmetrical shapes whereas fluvial transport equation may result in asymmetric behaviour because, locally, the direction of each bi-furcation of the fluvial network may be affected by negligibly small factors, even though the overall direction of the flow is controlled by the regional slope of topography

Although river networks in mountain ranges owe their existence to the competing effects of tectonic uplift and climate-controlled erosion, it was also argued that some universal geometric properties of river networks may be relatively independent of both tectonics and climate (Casteltort and Simpson, 2006). These authors have proposed that the geometry of river networks is established on the lowland margins of incipient uplifts, and is quenched into the erosion zone as the mountain belts widen with time. In that model, the geometry of river networks simply reflects the downward coalescence of alluvial rivers on undissected surfaces outside of mountain belts, and is therefore independent of erosion processes. Yet, the amount of the transported matter, incision rates, and other major dynamic parameters of the network are definitely tectonic-and-climate dependent.

3.2 Alternative Models of Surface Processes

The diffusion equation reflects an integrated effect of various processes acting at micro-and macroscale: chemical and physical erosion and weathering, gravity hillslope sliding etc. Some of these processes, for example, chemical erosion, are well described by the diffusion equation, since it reflects the physics of propagation of chemical interactions. On the other hand, gravity-driven processes are not diffusive. These processes are primarily slope dependent and thus do not fit well within the linear diffusion model (Densmore et al.,1997; 1998; Hasbargen and Paola, 2000; Roering et al., 2001; Schorghofer and Rothman, 2002; Pelletier, 2004). Indeed, it has been noted that the diffusion equation tends to over-smooth the predicted topography and fails to reproduce the usually sharp transitions from tectonically modified uplifted landscape to typically flat deposition surfaces in the foreland basins. To remedy this problem, either enhanced split (bi-mode) erosion models that discriminate between diffusion and gravity driven processes (e.g., Simpson and Schlunegger, 2003) or alternative stochastic (based on methods of artificial intellect such as cellular automates) and analogue models were proposed (Crave et al., 2000; Davy and Crave, 2000; Crave and Davy, 2001; Bonnet and Crave, 2003). Crave et al. (2001) or Tucker and Bras (1998; 2000), for example, used stochastic methods based on cellular automats that "learn" how to reproduce erosion/sedimentation from pre-imposed logical rules that establish relations between a given grid cell and its neighbors, as a function of the local slope, height, precipitation, regolith type and other conditions. If the rules and their rela-

tions are well established, they may form the "vocabulary" and "grammar" (= "language") for description of topography evolution. This approach may eventually produce more realistic landscapes than the common diffusion-fluvial transport models. However, for each new application, it requires one to justify the local applicability of the previously established rules. Analogue (physical) erosion models were used to study erosional response to tectonic forcing (e.g., Lague et al., 2003). These models may produce naturally looking landscapes, yet their applicability is rather limited since it is highly difficult to control, scale and interpret their parameters.

Linear and nonlinear diffusion short-range models combined with fluvial transport long-range models (Fig. 3) remain to be most widely used for tectonic-scale modelling. In particular, diffusion and fluvial transport equations can be generalized (Simpson and Schlunegger, 2003) as following:

$$\begin{cases} \dfrac{dh}{dt} = \nabla \cdot \left((k + cq^{n}) \nabla h \right) \\ \nabla \cdot \left(\dfrac{\nabla h}{|\nabla h|} q \right) = -\alpha \\ De = \dfrac{c\alpha^{n} L^{n}}{k} \end{cases} \tag{5}$$

where c is sediment discharge, α is effective rainfall, q is surface fluid discharge, and $k + cq^n$ has a sense of a variable nonlinear diffusion coefficient that incorporates both the effects of diffusion-driven (k-term: chemical and physical erosion, weathering) processes and gravity-driven, i.e. fluvial, processes (cq^n term: slope-dependent flow, sliding, creep etc). The respective role of dispersive processes and hillslope creep processes is characterized by dimensionless De number (L is characteristic length scale).

4 Structure and Rheology of the Lithosphere

4.1 Rheology

Many studies of the interplay between erosion and tectonics have been conducted assuming either local isostasy (Ahnert, 1970; Leeder, 1991) or thin plate flexural behavior of the lithosphere (Beaumont, 1981; Flemings and Jordan, 1989;1990; Beaumont et al., 1992; Masek et al., 1994a,b; Garcia-Castellanos, 2002; Garcia-Castellanos et al., 2002; Garcia-Castellanos et al., 2003). Some authors have considered the possibility for ductile flow in the lower crust and treated the lower crust as an inviscid fluid overlaid by a thin elastic plate (King et al., 1988; King and Ellis, 1990; Avouac and Burov, 1996; Burov and Cloetingh, 1997; Burov et al., 2001). The effect of variations in the surface loading and in the crustal thickness on the mechanical behavior of the lithosphere have been often neglected, except several studies (e.g., Beaumont et al., 1992, 2000; Avouac and Burov, 1996; Burov and Cloetingh, 1997; Burov et al., 2001; Toussaint et al., 2004a,b). The coupled erosion-tectonics regime described in the previous sections assumes that strain localization below a tectonic load, range or basin, results from weakening of the lithosphere due to crustal thickening and bending stresses. In order to account for this process one can treat the lithosphere neither as a one-layer elastic or visco-elastic plate with vertically integrated properties overlying an inviscid asthenosphere, or as a thin viscous sheet (e.g., England and McKenzie, 1983; Vilotte et al., 1982). We thus have to consider the lithological and mechanical rheological layering of the lithosphere. For the model demonstrated here, three lithological layers were defined: the upper crust, the lower crust, and the mantle (Fig. 2a). Each layer has specific properties (density, mechanical, and thermal constants) that are given in Table 1. We assume no compositional changes due to deformation or cooling. The lithological boundary between the upper and lower crust lies at a fixed depth of 20 km. The bottom of the mantle lithosphere is limited by the 1330°C isotherm at a depth of about 250 km. At small differential stresses the rocks behave elastically. In terms of principal components, the relationship between the stress tensor, σ, and the strain tensor, ε, can be written:

$$\sigma_j = 2\mu_e \varepsilon_j + \lambda(\varepsilon_1 + \varepsilon_2 + \varepsilon_3) \tag{6}$$

where j =1, 2, 3. λ and μ_e are Lamé's constants related to Young's modulus (E) and Poissons's ratio ν as $\lambda = E\,\nu((1+\nu)(1-2\nu))^{-1}$; $\mu_e = E/2(1+\nu)$. Typical values for E and ν are $6.5–8\times10^{10}$ N/m^2 and 0.25, respectively (e.g., Turcotte and Schubert, 1982).

Weakening by brittle failure or ductile flow occurs when elastic stresses reach some threshold value that determines the condition for failure or significant ductile deformation. Above this threshold rocks no longer behave elastically, and unrecoverable strain may grow without increase of stress. The conditions of brittle failure are independent of rock type and temperature, but strongly controlled by pressure (Byerlee, 1978):

$$\begin{aligned} &\sigma_3 = (\sigma_1 - \sigma_3)/3.9 \text{ at } \sigma_3 < 120 \text{ MPa}; \\ &\sigma_3 = (\sigma_1 - \sigma_3)/2.1 - 100 \text{ MPa at } \sigma_3 \geq 120 \text{ MPa} \end{aligned} \tag{7}$$

where σ_1, σ_2, σ_3 are principal stresses [MPa]. This law corresponds to Mohr-Coulomb plastic behavior.

Ductile flow in the lithosphere essentially results from dislocation creep (e.g., Kusznir, 1991). This

Table 1a. Definition of variables

Variable	Values and units	Definition	Comments
τ_{xx}, τ_{xy}, τ_{yy},	Pa, MPa	shear stress components	
σ_{xx}, σ_{xy}, σ_{yy}	Pa, MPa	full stress components	$\boldsymbol{\sigma} = \tau - P\mathbf{I}$, $\sigma_{xy} = \tau_{xy}$ etc.
P	Pa, MPa	pressure	
$\mathbf{v}$	m/s, mm/y	total velocity vector	
u	m/s, mm/y	horizontal velocity	x component of v
v	m/s, mm/y	vertical velocity	y component of v
μ	Pa s	effective viscosity	10^{19} to 10^{25} Pa s
k	m^2 / y	coefficient of erosion	~ mass diffusivity
dh	m, km	topographic uplift	or subsidence
du	m, km	tectonic uplift	do not mix with u
de	m, km	erosion	or sedimentation
ψ	m^2/s	stream function	$v = \partial\psi / \partial y, v = \partial\psi / \partial y$
ξ	s^{-1}	vorticity function	$\partial v / \delta y - \partial v / \partial x = \Delta\psi$
ε		strain	
$\dot{\varepsilon}$	s^{-1}	average strain rate	$\dot{\varepsilon} = (½\, \dot{\varepsilon}_{ij} \dot{\varepsilon}_{ij})^{½}$
q	m^2/s	integrated flux	ductile crust
q_e	(m^2/s) / m	erosional flux	per unit length
E	$8{\times}10^{10}$ N/m^2	Young's modulus	in the semi-analytical model
v	0.25	Poisson's ratio	in the semi-analytical model
λ, μ_e	N/m^2	Lamé's constants	
A^*	Pa^{-n} s^{-1}	material constant	power law
n	3 to 5	stress exponent	power law
H^*	kJ mol^{-1}	activation enthalpy	power law
R	8.314 J/mol K	gas constant	power law
T	C°, K	temperature	
$\gamma(y)$	Pa/m, MPa/km	depth gradient of yield stress	$\gamma(y) \propto d\sigma(\varepsilon)/dy$,
w	m, km	plate deflection	~ deflection of mantle lithosphere
T_e, $\tilde{T}_e(x, w, w', w'', t)$	m, km	effective elastic thickness	~ instant integrated strength
T_{ec}	m, km	effective elastic thickness of the crust	$T_e \approx (T_{ec}^3 + T_{em}^3)^{1/3}$ $T_{ec} \le h_{c_1}$
T_{em}	m, km	effective elastic thickness of mantle lithosphere	$T_e \approx (T_{ec}^3 + T_{em}^3)^{1/3}$ $T_{em} \le h_{c_2} - T_c$
$\tilde{M}_x$	N m / m	flexural moment	per unit length
$\tilde{T}_x$	N	longitudinal force	
$\tilde{Q}_x$	N / m	shearing force	per unit length
p^+	Pa, N/m^2	surface load	
p^-	Pa / m	restoring stress	per unit length
$h(x, t)$	m, km	surface topography	
$\tilde{h}(x, t)$	m, km	upper boundary of ductile channel	
h_c, T_c	m, km	Moho depth	Moho boundary
h_{c_2}	m, km	lower boundary of ductile crustal cannel	$h_{c_2} \le T_c$

Table 1a. *Continued*

Variable	Values and units	Definition	Comments
$h_{c_1}(x, t, w)$	m, km	maximal mechanical thickness of the upper crust	here, 10–20 km depending on stress
$\Delta h_{c_2}(x, t, w, u, v)$	m, km	thickness of crustal channel	
y_{ij}	m, km	depths to lithological and mechanical interfaces	*i* is number of a detached layer *j* is number of the mechanical sub-layer
ρ_{c_1}	2650 kg/m^3	density	of upper crust
ρ_{c_2}	2900 kg/m^3	density	of lower crust
ρ_m	3330 kg/m^3	density	of mantle
α	degrees	inclination of upper boundary of channel	$\alpha \sim \partial\tilde{h} / \partial x$
β	degrees	inclination of lower boundary of channel	$\beta \sim \partial w / \partial x$
g	9.8 m/s^2	acceleration due to gravity	
T	°C	temperature	
t_a	m.y.	thermal age	≤ geological age
a	250 km	thermal thickness of the lithosphere	
T_m	1330 °C	T at depth a	
χ	m^{2}s^{-1}	thermal diffusivity	$\chi = k/\rho C_p$
χ_{c_1}	8.3×10^{-7} m^{2}s^{-1}	thermal diffusivity	upper crust
χ_{c_2}	6.7×10^{-7} m^{2}s^{-1}	thermal diffusivity	lower crust
χ_m	8.75×10^{-7} m^{2}s^{-1}	thermal diffusivity	mantle
k_{c_1}	2.5 Wm^{-1}°K^{-1}	thermal conductivity	upper crust
k_{c_2}	2 Wm^{-1}°K^{-1}1	thermal conductivity	lower crust
k_m	3.5 Wm^{-1}°K^{-1}	thermal conductivity	mantle
h_r	10 km	decay scale of radiogenic heat production	upper crust
H_s	9.5×10^{-10} W kg^{-1}	surface radiogenic heat pro-duction rate per unit mass	upper crust
$H_{c_2} C_{c_2}^{-1}$	1.7×10^{-13}°K s^{-1}	radiogenic heat	lower crust
ρC_p	J (m^{3}K)$^{-1}$	density × specific heat	

mechanism is thermally activated and results in relationship between strain rate and stress which can be written:

$$\dot{\varepsilon} = A^* \exp(-H^*/RT)\ (\sigma_1 - \sigma_3)^n \qquad (8)$$

The material constants adopted for the creep law of lithospheric minerals are given in 1b. The ratio of the stress to strain rate defines an effective non-Newtonian viscosity:

$$\mu_{\text{eff}} = \left(\frac{\partial \varepsilon}{\partial t}\right)_{\text{II}}^{d^{(1-n)/n}} (A^*)^{-1/n} \exp\left(H/nRT\right) \qquad (9)$$

where $\left(\frac{\partial \varepsilon}{\partial t}\right)_{\text{II}}^{d} = \left(Inv_{\text{II}}\left(\frac{\partial \varepsilon_{ij}}{\partial t}\right)\right)^{1/2}$

is the effective strain rate and $A^* = \frac{1}{2}A \cdot 3^{(n+1)/2}$ is the material constant, H is the activation enthalpy, R is the gas constant, n is the power law exponent. Although

Table 1b. Summary of rheology parameters used in model calculations

Parameter	Value
Lamé elastic constants $\lambda = G$	30 GPa (in numerical models)
Friction angle (Mohr-Coulomb criterion)	30°
Cohesion (Mohr-Coulomb criterion)	20 Mpa
Specific upper and weak lower-crust properties	
ρ (upper crust)	2800 kg m^{-3}
ρ (lower crust)	2900 kg m^{-3}
n	2.4
A	6.7×10^{-6} MPa–n·s^{-1}
Q	1.56×10^{5} kJ·mol^{-1}
Specific strong lower-crust properties	
ρ	2980 kg m^{-3}
n	3.4
A	2×10^{-4} MPa^{-n}·s^{-1}
Q	2.6×10^{5} kJ·mol^{-1}
Specific mantle properties	
ρ (lithosphere)	3330 kg m^{-3}
ρ (oceanic slab)	3350 kg m^{-3}
ρ (asthenosphere)	3310 kg m^{-3}
n	3
A	1×10^{4} MPa^{-n}·s^{-1}
Q	5.2×10^{5} kJ·mol^{-1}

Note: Compilation by Burov et al. [2001]. Q, n, A are parameters of the ductile flow law (activation energy, material constant, and power exponent, respectively). See also [Brace and Kohlstedt, 1980; Kirby, 1983; Kirby and Kronenberg, 1987; Kohlsted et al., 1995; Byerlee, 1978; Carter and Tsenn, 1987; Tsenn and Carter, 1987]

ductile deformation occurs even under low differential stresses, a ductile yield strength can be defined. If boundary conditions are given in terms of rate of displacement, a "basic" strain rate can be derived and represents the average strain rate in the medium (10^{-15} s^{-1} – 5×10^{-15} s^{-1}). This "basic" strain rate corresponds to a stress threshold defined from Eq. (8). Owing to the nonlinearity of rheology described by Eq. (8) the ductile deformation will process very slowly so that most of the imposed deformation will be absorbed elastically if the stress is slightly less than the yield level. For example, for olivine, strain rate decreases by a factor of 1000 if the stress lies 10–15% below the "threshold" level. This behavior differs from that of a Newtonian fluid where decrease in stress would lead to a directly proportional decrease of the strain rate. On the opposite, the stress level cannot exceed significantly this threshold since it would require a strain rate much higher that the one that is imposed from boundary conditions. This threshold thus defines a ductile yield strength. A temperature of about 250–300°C must be exceeded for ductile deformation of quartz, whereas for olivine it should be 600–700°C (e.g., Brace and Kohlstedt, 1980; Carter and Tsenn, 1987; Kohlsted et al., 1995). It results in the yield stress envelope (YSE) being controlled by the conditions for brittle failure in the shallow crust and upper mantle, and by the condition for ductile failure in the deep crust and deep upper mantle. Combining rheological laws, Eqs. (6) to (9), form a piece-wise continuous yield-stress envelope (YSE) in $\Delta\sigma$-y space (Figure 2a, defined as a contour $\sigma^f = \sigma^f(x, y, t, \dot{\varepsilon})$ such that:

$$\sigma^f = sign(\varepsilon)\ \mathbf{min}(|\sigma^b(x, y, t, \dot{\varepsilon}, sign(\varepsilon))|, |\sigma^d(x, y, t, \dot{\varepsilon})|) \tag{10}$$

where $\sigma^b(x, y, t, \dot{\varepsilon}, sign(\varepsilon))$, $\sigma^d(x, y, t, \dot{\varepsilon})$ are the "brittle" and "ductile" yield stresses from Eqs. (6) and (7). sign(ε)=1 if $\varepsilon \geq 0$ and –1 if $\varepsilon < 0$. The differential stress $\sigma(x,y)$ at a point is taken to be equal to the minimum of σ^e and σ^f, computed as a function of the local strain $\varepsilon = \varepsilon(x, y, t, \dot{\varepsilon})$:

$$\sigma(\varepsilon) = \text{sign}(\varepsilon)\ \mathbf{min}(|\sigma^f|, |\sigma^e(\varepsilon)|) \tag{11}$$

where $\sigma^e(\varepsilon)$ is the elastic differential stress according to Eq. (5). If σ^e exceeds σ^f, the material is considered as ductile or brittle, depending on which rheology limits the yield strength. Due to asymmetry of the Byerlee's law (7), the yield stress depends on the mode of deformation, sign(ε) (for extension sign(ε)=1; for compression sign(ε)=–1). Equation (11) implies that the lithosphere remains elastic if imposed stress does not exceed the yield stress. Most of the upper crust remains elastic or brittle-elastic (depth interval between approx. 5 and 15–20 km). The crust is mostly ductile below 15–20 km. Depending on the geotherm and strain rates, first 30 to 70 km of the mantle lithosphere remains elastic. This formulation reflects the fact that the lithosphere gets weaker when submitted to increasing horizontal forces or flexural stresses and when the crust gets thicker.

4.2 Thermal Model

A thermal model is required to define the rheological profile of the lithosphere and to fully account for the effect of crustal thickening on the rheology of the lithosphere. In this paper, the initial geotherm is computed according to a half-space heat transfer model (for details see Burov et al., 1993 and Burov and Diament, 1995). For the following evolution, heat transfer equations are solved separately for the upper crust, lower

crust, and mantle with conditions of temperature and heat flux continuity across the interfaces. These equations have the form:

$$\dot{T} + uT_x' + vT_y' - \chi_f \Delta T = H_d + H_r + v\Omega \quad (12)$$

where primes mean spatial differentiation by respective coordinate. The thermal diffusivity parameter χ_f equals to χ_{c1}, χ_{c2}, χ_m depending on the lithological layer (see Table 1). $H_r = \chi_{c1} k_{c1}^{-1} \rho_c H_s \exp(-yh_r^{-1})$ is the radiogenic heat. H_r equals to constant heat generation $H_{c2} C_{c2}^{-1}$ in the lower crust and to zero in the mantle. H_d refers to heat generation due to mechanical dissipation (e.g., frictional heating). The adiabatic temperature gradient in the asthenosphere, Ω, is 0.3°C/km (Turcotte and Schubert, 1982).

The boundary and initial conditions are: $T(x,0,t_a) =$ 0°C (temperature at the upper surface = const at time t_a, where t_a is the thermal age); $T(x,a,t) = T_m = 1350$°C ($a \approx 250$ km is the depth to the thermal bottom, or thermal thickness of the lithosphere); $T(x,y,0) = T_m$ (homogeneous temperature distribution at the beginning). t_a is defined as the age of the last large-scale thermal event determined from geological data.

5 Implementation of Coupled Models

5.1 Semi-Analytical Model

In this section we describe the numerical procedure used in the semi-analytical model by Avouac and Burov (1996) and Burov and Cloetingh (1997).

In this model, we distinguish between competent and weak layers (Fig. 4, top). The competent layers are those which contribute significantly to the flexural strength of the lithosphere. This encompasses not only the elastic domains but also high stress (>5% of the lithostatic pressure) brittle and ductile domains (e.g., Burov and Diament, 1992; 1995). Only the competent

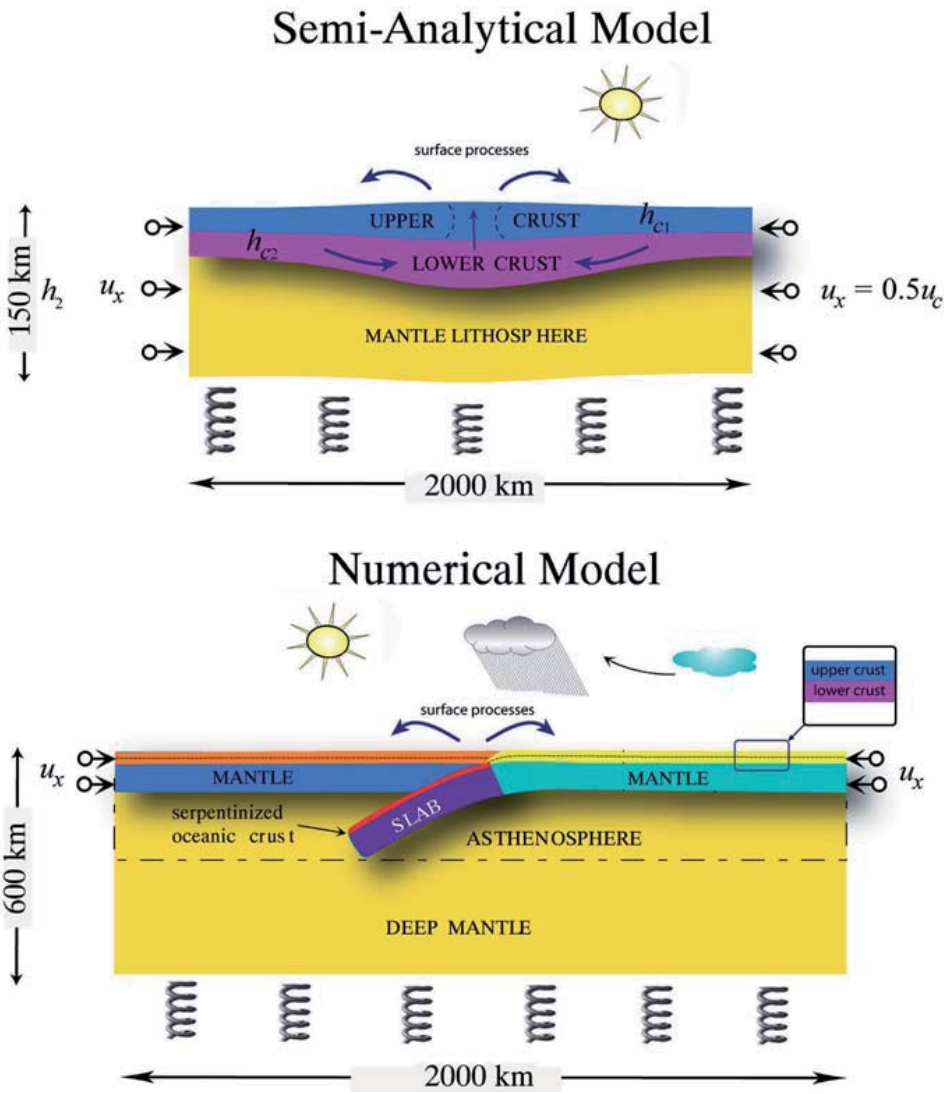

Fig. 4. Model Setups. Top: Setup of a simplified semi-nalytical collision model with erosion-tectonic coupling (Avouac and Burov, 1996). In-eastic flexural model is used to for competent parts of crust and mantle, channel flow model is used for ductile domains. Both models are coupled via boundary conditions. The boundaries between competent and ductile domains are not predefined but are computed as function of bending stress that conrols brittle-ductile yielding in the lithosphere. Diffusion erosion and flat deposition are imposed at surface. In these experiments, initial topography and isostatic crustal root geometry correspond to that of a 3 km high and 200 km wide Gaussian mount.Bottom. Setup of fully coupled thermo-mechanical collision-subduction model (Burov et al., 2001; Toussaint et al., 2004b). In this model, topography is not predefined and deformation is solved from full set of equilibrium equations. The assumed rheology is brittle-elastic-ductile, with quartz-rich crust and olivine-rich mantle (Table 1)

layers are considered in the computation of the flexural response of the lithosphere. The geometry and thickness of the mechanical layers depend on the lithological layering and on the stress field. Since both evolve during the numerical experiment, the mechanical structure is re-computed at each numerical step. Vertical deflections (w) of the competent portions of the crust and mantle lithosphere due to change in the stress applied at their boundaries are treated as instantaneous deflections of flexible layers [Appendix A]. Deformation of the ductile crust, driven by the deflection of the competent layers that bound the low viscosity lower crustal channel, is modelled as a flow of a non-Newtonian fluid in a channel of variable thickness. No horizontal flow at the axis of symmetry of the range ($x = 0$) is allowed. Away from the mountain range, where the channel has a nearly constant thickness, the flow is computed according to the thin channel approximation [Appendix B]. Since the conditions for this approximation are not satisfied in the thickened region, we use a semi-analytical solution for the ascending flow fed by remote channel source [Appendix C]. The distance al at which the channel flow approximation is replaced by a formulation for the ascending flow, equals to 1 to 2 thicknesses of the channel, depending on the integrated strength of the upper crust [Appendixes B and C]. Since the common brittle-elastic-dutile rheology profiles imply decoupling between the mantle and crust [Fig. 2a], in particular where the crust is thick, deformation of the crust is expected to be relatively insensitive to what happens in the mantle. Shortening of the mantle lithosphere is therefore neglected. Naturally, this assumption will not directly apply if partial coupling of mantle and crustal lithosphere occurs (e.g., Ter Voorde et al., 1998; Gaspar-Escribano et al., 2003). For this reason, in the next sections, we present a less constrained fully numerical model, in which the conditions on the crust-mantle interface are not pre-described.

The various equations define the mechanical structure of the lithosphere, flexure of the competent layers, ductile flow in the ductile crust, erosion and sedimentation at the surface are solved at each numerical iteration as depicted in the following flow-chart:

see Box 1, Eq. 13

B.C. and I.C. refer to boundary and initial conditions, respectively. Notation (k) implies that related value is used on k-th numerical step. Notation (k–1) implies that the value is taken as a predictor from the previous time step, etc. All variables are defined in Table 1. The following continuity conditions are satisfied at the interfaces between the competent layers and the ductile crustal channel:

see Box 1, Eq. 14

Box 1.
Eq. 13 + 14

Input → Output

$$
\begin{cases}
\text{I. } u_{k-1}, v_{k-1}, T_{c\,(k-1)}, w_{k-1}, h_{k-1} \\
\quad + B.C.\&I.C._k \rightarrow (\text{A1, 12, 14}) \rightarrow T \\
\text{II. } T, \dot{\varepsilon}, A, H^*, n, T_{c(k-1)} \rightarrow (6\text{–}11) \rightarrow \sigma^f, h_{c1}, h_{c2}, h_m \\
\text{III. } \sigma^f, h_{c1}, h_{c2}, h_m, h_{k-1}, \\
\quad p^-_{k-1}, p^+_{k-1} + B.C._k \rightarrow (\text{A1}) \rightarrow w_k, T_{c(k)}, \sigma(\varepsilon), y_{ij_{(k)}} \\
\text{IV. } w_k, \sigma(\varepsilon), y_{ij_{(k)}}, \tilde{h}_{k-1}, \sigma^f, \\
\quad \dot{\varepsilon}, h_{k-1}, T_{ck} + B.C._k \rightarrow (\text{B5, B6, C3}) \rightarrow u_k, v_k, \tilde{h}_k, h_k, T_{ck+1}, \tau_{xy}, \delta T_1 \\
\text{V. } h_k, (\text{i.e., } I.C._k) \rightarrow (3\text{–}4) \rightarrow h_{k+1}, \delta T_2
\end{cases}
\tag{13}
$$

$$
\begin{aligned}
&\textit{continuity of vertical velocity} && v^-_{c1} = v^+_{c2};\ v^-_{c2} = v^+_m \\
&\textit{continuity of normal stress} && \sigma^-_{yy_{c1}} = \sigma^+_{yy_{c2}};\ \sigma^-_{yy_{c2}} = \sigma^+_{yy_m} \\
&\textit{continuity of horizontal velocity} && u^-_{c1} = u^+_{c2};\ u^-_{c2} = u^+_m \\
&\textit{continuity of the tangential stress} && \sigma^-_{xy_{c1}} = \sigma^+_{xy_{c2}};\ \sigma^-_{xy_{c2}} = \sigma^+_{xy_m} \\
&\textit{kinematic condition} && \frac{\partial \tilde{h}}{\partial t} = v^+_{c2};\ \frac{\partial w}{\partial t} = v^-_{c2}
\end{aligned}
\tag{14}
$$

Superscripts "+" and "–" refer to the values on the upper and lower interfaces of the corresponding layers, respectively. The subscripts c_1, c_2, and m refer to the strong crust ("upper"), ductile crust ("lower") and mantle lithosphere, respectively. Power-law rheology results in self-lubrication and concentration of the flow in the narrow zones of highest temperature, that is near the Moho. For this reason, there is little difference between the assumption of no-slip and free slip boundary for the bottom of the ductile crust.

The spatial resolution used for calculations is $dx = 2$ km, $dy = 0.5$ km. The requirement of stability of integration of the diffusion equations (3), (4) ($dt < 0.5dx^2/k$) implies a maximum time step of < 2000 years for $k = 10^3$ m^2/y and of 20 years for k = 10^5 m^2/y. It is less than the relaxation time for the lowest viscosity value (~ 50 years for = 10^{19} Pa s). We thus chose a time step of 20 years in all semi-analytical computations.

5.2 Unconstrained Fully Coupled Numerical Model

To fully demonstrate the importance of interactions between the surface processes, ductile crustal flow and major thrust faults, and also to verify earlier ideas on evolution of collision belts, we used fully coupled (mechanical behavior - surface processes - heat transport) numerical models, which combine brittle-elastic-ductile rheology and account for large strains, fault localization, and erosion/sedimentation mechanisms (Fig. 4, bottom).

We have extended the Paro(a)voz code (Polyakov et al., 1993, Appendix D) based on the FLAC (Fast Langrangian Analysis of Continua) algorithm (Cundall, 1989). This "2.5 D" explicit time-marching, large-strain Lagrangian algorithm locally solves Newtonian equations of motion in continuum mechanics approximation and updates them in large-strain mode. The particular advantage of this code refers to the fact that it operates with full stress approximation which allows for simple and accurate computation of total pressure, P, as a trace of the full stress tensor. The solution of these equations is coupled with those of constitutive and heat-transfer equations. Parovoz v9 is thus a fully thermally coupled code that also handles explicit elastic-ductile-plastic rheologies, free-surface boundary conditions, full metamorphic changes, and surface processes (erosion and sedimentation). The Lagrangian numerical mesh, which periodically becomes distorted and thus needs remeshing, is doubled by a denser passive marker grid allowing to interpolate grid values, specifically stresses, with minimal losses during remeshing.

We test continental collision assuming acommonly referred initial scenario (Fig. 4, bottom), in which (1) the rapidly subducting oceanic slab first entrains a very small part of a cold continental "slab" (there is no continental subduction at the beginning), and (2) the initial convergence rate equals to or is smaller than the rate of the preceding oceanic subduction (two-sided initial closing rate of 2×6 mm/y during 50 My for Alpine collision test (Burov et al., 2001) or 2×3 cm/y during the first 5–10 My for the India-Asia collision test (Toussaint et al., 2004b). The rate chosen for the India-Asia collision test is smaller than the average historical convergence rate between India and Asia (2×4 to 2×5 cm/y during the first 10 My. (Patriat and Achache, 1984).

For continental collision models, we use commonly inferred crustal structure and rheology parameters derived from rock mechanics (Table 1; Burov et al., 2001). The thermo-mechanical part of the model that computes, among other parameters, the upper free surface, is coupled with the surface process model based on the diffusion equation (4a). On each type step the geometry of the free surface is updated with account for erosion and deposition. The surface areas affected by sediment deposition change their material properties according to those prescribed for sedimentary matter (Table 1). In the experiments shown below, we used linear diffusion with a diffusion coefficient that has been varied from 0 to 2000 m^2/y (Burov et al., 2001). The initial geotherm was derived from the common half-space model (e.g., Parsons and Sclater, 1977) as discussed in the section "Thermal mode" and Appendix D.

The universal controlling variable parameter of all continental experiments is the initial geotherm (Fig. 2a), or thermotectonic age (Turcotte and Schubert, 1982), identified with the Moho temperature Tm. The geotherm or age defines major mechanical properties of the system, e.g., the rheological strength profile (Fig. 2a). By varying the geotherm, we can account for the whole possible range of lithospheres, from very old, cold, and strong plates to very young, hot, and weak ones. The second major variable parameter is the composition of the lower crust, which, together with the geotherm, controls the degree of crust-mantle coupling. We considered both weak (quartz dominated) and strong (diabase) lower-crustal rheology and also weak (wet olivine) mantle rheology (Table 1). Although we mainly applied a convergence rate of 2 × 3 cm/y, we also tested smaller convergence rates (two times smaller, four times smaller, etc.).

6 Experiments

6.1 Semi-Analytical Model

Avouac and Burov (1996) have conducted series of experiments, in which a 2-D section of a continental lithosphere, loaded with some initial range (resembling an averaged cross-section of Tien Shan), is submitted to horizontal shortening (Fig. 4, top) in pure shear mode. Our goal was to validate the idea of the coupled (erosion-tectonics) regime and to check whether it can allow for stable localized mountain growth. Here we were only addressing the problem of the growth and maintenance of a mountain range once it has reached some mature geometry.

We thus consider a 2000-km-long lithospheric plate initially loaded by a topographic irregularity. Here we do not pose the question how this topography was formed, but in later sections we show fully numerical experiments, in which the mountain range grows from initially flat surface. We chose a 300–400-km-wide "Gaussian" mountain (a Gaussian curve with variance 100 km, that is about 200 km wide). The model range has a maximum elevation of 3000 m and is initially regionally compensated. The thermal profile used to compute the rheological profile corresponds approximately to the age of 400 My. The initial geometry of the Moho was computed from the flexural response of the competent cores of the crust and upper mantle and neglecting viscous flow in the lower crust (Burov et al., 1990). In this computation, the possibility of the internal deformation of the mountain range or of its crustal root was neglected. The model is then submitted to horizontal shortening at rates from about 1 mm/y to several cm/y. These rates largely span the range of most natural large-scale examples of active intracontinental mountain range. Each experiment modelled 15–20 My of evolution with time steps of 20 years. The geometries of the different interfaces (topography, upper-crust-lower crust, Moho, basement-sediment in the foreland) were computed for each time step. We also computed the rate of uplift of the topography, dh/dt, the rate of tectonic uplift or subsidence, du/dt, the rate of denudation or sedimentation, de/dt, (Fig. 5), stress, strain and velocity field. The relief of the range, Δh, was defined as the difference between the elevation at the crest $h(0)$ and in the lowlands at 500 km from the range axis, $h(500)$.

In the case where there are no initial topographic or rheological irregularities, the medium has homogeneous properties and therefore thickens homogeneously (Fig. 5b). There are no horizontal or vertical gradients of strain so that no mountain can form. If the medium is initially loaded with a mountain range, the flexural stresses (300–700 MPa; Fig. 5a) can be 3–7 times higher than the excess pressure associated with the weight of the range itself (~100 MPa). Horizontal

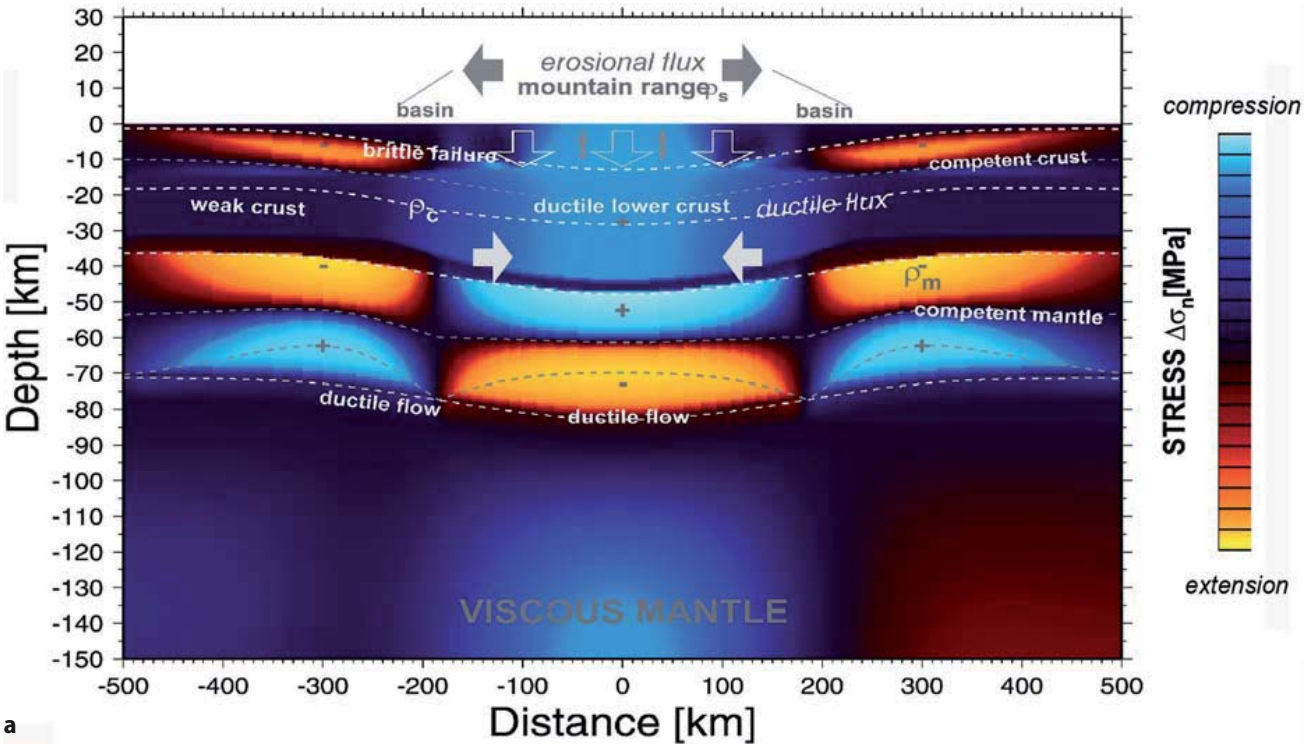

Fig. 5a. Example of normalized stress distribution in a semi-analytical experiment in which stable growth of the mountain belt was achieved (total shortening rate 44 mm/y; strain rate 0.7×10^{-15} sec^{-1} erosion coefficient 7500 m^2/y

shortening of the lithosphere tend therefore to be absorbed preferentially by strain localized in the weak zone beneath the range. In all experiments the system evolves very rapidly during the first 1–2 million years because the initial geometry is out of dynamic equilibrium. After the initial reorganization, some kind of dynamic equilibrium is reached, in which the viscous forces due to flow in the lower crust also participate in the support of the surface load.

6.1.1 Case 1: No Surface Processes: "Subsurface Collapse"

In the absence of surface processes the lower crust is extruded from under the high topography (Fig. 5b). The crustal root and the topography spread out laterally. Horizontal shortening leads to general thickening of the medium but the tectonic uplift below the range is smaller than below the lowlands so that the relief of the range, Δh, decays with time. The system thus evolves towards a regime of homogeneous deformation with a uniformly thick crust. In the particular case of a 400-km-wide and 3-km-high range it takes about 15 My for the topography to be reduced by a factor of 2. If the medium is submitted to horizontal shortening, the decay of the topography is even more rapid due to in-elastic yielding. These experiments actually show that assuming a common rheology of the crust without intrinsic strain softening and with no particular assumptions for mantle dynamics, a range should collapse in the long term, as a result of subsurface deformation, even the lithosphere undergoes intensive horizontal shortening. We dubbed "subsurface collapse" this regime in which the range decays by lateral extrusion of the lower crustal root.

6.1.2 Case 2: No Shortening: "Erosional Collapse"

If erosion is intense (with values of k of the order of 10^4 m^2/y) while shortening is slow, the topography of the range vanishes rapidly. In this case, isostatic readjustment compensates for only a fraction of denudation and the elevation in the lowland increases as a result of overall crustal thickening (Fig. 5b). Although the gravitational collapse of the crustal root also contributes to the decay of the range, we dubbed this regime "erosional", or "surface" collapse. The time constant associated with the decay of the relief in this regime depends on the mass diffusivity. For $k = 10^4$ m^2/y, denudation rates are of the order of 1 mm/y at the beginning of the experiment and the initial topography was halved in the first 5 My. For $k = 10^3$ m^2/y the range topography is halved after about 15 My. Once the crust and Moho topographies have been smoothed by surface processes and subsurface deformation, the system evolves towards the regime of homogeneous thickening.

6.1.3 Case 3: Dynamically Coupled Shortening and Erosion: "Mountain Growth"

In this set of experiments, we started from the conditions leading to the "subsurface collapse" (significant shortening rates), and then gradually increased the intensity of erosion. In the experiments where erosion was not sufficiently active, the range was unable to grow and decayed due to subsurface collapse. Yet, at some critical value of k, a regime of dynamical coupling was reached, in which the relief of the range was growing in a stable and localized manner (Fig. 5b, bottom). Similarly, in the other set of experiments, we started from the state of the "erosional collapse", kept the rate of erosion constant, and gradually increased the rate of shortening. At low shortening rates, erosion could still erase the topography faster then it was growing, but at some critical value of the shortening rate, a coupled regime was reached (Figs. 5a, 5b). In the coupled regime, the lower crust was flowing towards the crustal root (inward flow) and the resulting material in-flux exceeded the amount of material removed from the range by surface processes. Tectonic uplift below the range then could exceed denudation (Fig. 5) so that the elevation of the crest was increasing with time. We dubbed this regime "mountain growth". The distribution of deformation in this regime remains heterogeneous in the long term. High strains in the lower and upper crust are localized below the range allowing for crustal thickening (Fig. 5a). The crust in the lowland also thickens owing to sedimentation but at a smaller rate than beneath the range. Figure 5b shows that the rate of growth of the elevation at the crest, dh/dt (x=0), varies as a function of time allowing for mountain growth. It can be seen that "mountain growth" is not monotonous and seems to be very sensitive, in terms of surface denudation and uplift rate, to small changes in parameters. However, it was also found that the coupled regime can be self-maintaining in a quite broad parameter range, i.e., erosion automatically accelerates or decelerates to compensate eventual variations in the tectonic uplift rate (Fig. 5c). Figure 5c shows that the feedback between the surface and subsurface processes can maintain the mountain growth regime even for large deviations of k_s and $\partial\varepsilon_{xx}/\partial t$ from the equilibrium state. These deviations may cause temporary oscillations in the mountain growth rate (curves 2 and 3 in Figure 5c) that are progressively damped as the system finds a new stable regime. These experiments suggest that orogenic systems may be quite resistant to climatic changes or variations in tectonic rates, yet they may very rapidly

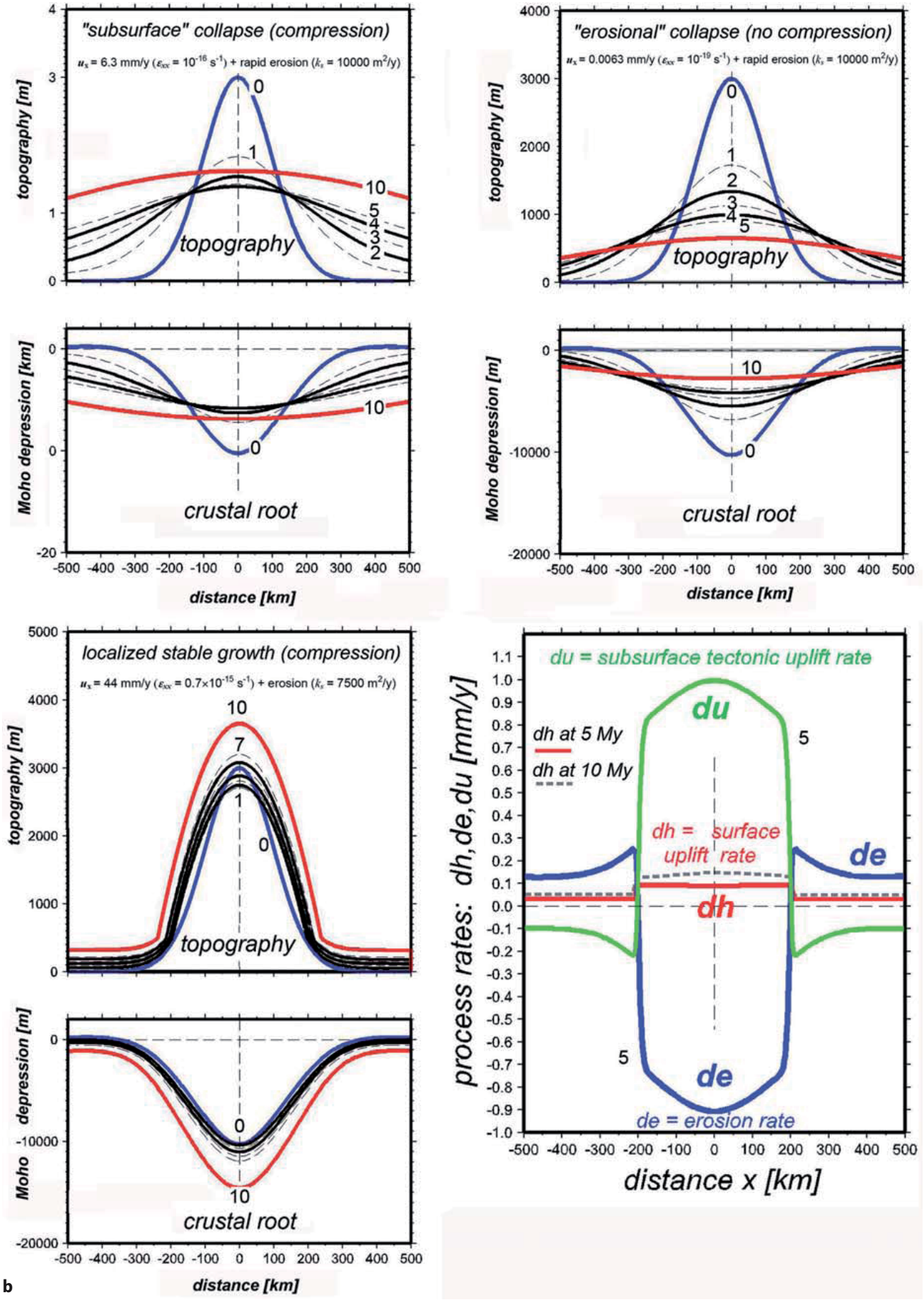
"subsurface" collapse (compression)
u_x = 6.3 mm/y (ε_{xx} = 10^{-16} s^{-1}) + rapid erosion (k_s = 10000 m^2/y)
topography [m]
topography
Moho depression [km]
crustal root
distance [km]
"erosional" collapse (no compression)
u_x = 0.0063 mm/y (ε_{xx} = 10^{-19} s^{-1}) + rapid erosion (k_s = 10000 m^2/y)
topography [m]
topography
Moho depression [m]
crustal root
distance [km]
localized stable growth (compression)
u_x = 44 mm/y (ε_{xx} = 0.7×10^{-15} s^{-1}) + erosion (k_s = 7500 m^2/y)
topography [m]
topography
Moho depression [m]
crustal root
distance [km]
du = subsurface tectonic uplift rate
du
dh at 5 My
dh at 10 My
dh = surface uplift rate
de
dh
de
de = erosion rate
process rates: dh,de,du [mm/y]
distance x [km]

b

◀ **Fig. 5b.** Results of representative semi-analytical experiments: topography and crustal root evolution within first 10 My, shown with interval of 1 My. Top, right: Gravity, or subsurface, collapse of topography and crustal root (total shortening rate 2×6.3 mm/y; strain rate 10^{-16} s^{-1} erosion coefficient 10000 m^2/y). Top, left: erosional collapse (total shortening rate 2× 0.006.3 mm/y; strain rate 10^{-19} s^{-1} erosion coefficient 10000 m^2/y). Bottom, left: Stable localised growth of the topography in case of coupling between tectonic and surface processes observed for total shortening rate 44 mm/y; strain rate 0.7×10^{-15} s^{-1} erosion coefficient 7500 m^2/y. Bottom, right: distribution of residual surface uplift rate, dh, tectonic uplift rate, du, and erosion-deposition rate de for the case of localised growth shown at bottom, left. Note that topography growth in a localized manner for at least 10 My and the perfect anti-symmetry between the uplift and erosion rate that may yield very stable steady surface uplift rate

collapse if the limits of the stability range are exceeded (curves 3,4 in Fig. 5c). We did not further explore the dynamical behavior of the system in the coupled regime but we suspect a possibility of chaotic behaviors, hinted, for example, by complex oscillations in case 3 (Fig. 5c). Such chaotic behaviours are specific for feedback-controlled systems in case of delays or other changes in the feedback loop. This may refer, for example, to the delays in the reaction of the crustal flow to the changes in the surface loads; to a partial loss of the sedimentary matter from the system (long-distance fluvial network or out of plain transport); to climatic changes etc.

Figure 6 shows the range of values for the mass diffusivity and for the shortening rate that can allow for the dynamical coupling and thus for mountain growth. As a convention, a given experiment is defined to be in the "mountain growth" regime if the relief of the range increases at 5 My, which means that elevation at the crest ($x = 0$) increases more rapidly than the elevation in the lowland ($x = 500$ km):

$$dh/dt\ (x{=}0\,\text{km}) > dh/dt\ (x{=}500\,\text{km})\ \text{at}\ t{=}5\,\text{My} \qquad (15)$$

As discussed above, higher strain rates lead to reduction of the effective viscosity (μ_{eff}) of the non-Newtonian lower crust so that a more rapid erosion is needed to allow the feedback effect due to surface processes. Indeed, μ_{eff} is proportional to $\dot{\varepsilon}^{1/(n-1)}$. Taking into account that n varies between 3 and 4, this provides a half-order decrease of the viscosity at one-order increase of the strain rate from 10^{-15} to 10^{-14} s^{-1}. Consequently, the erosion rate must be several times higher or slower to compensate 1 order increase or decrease in the tectonic strain rate.

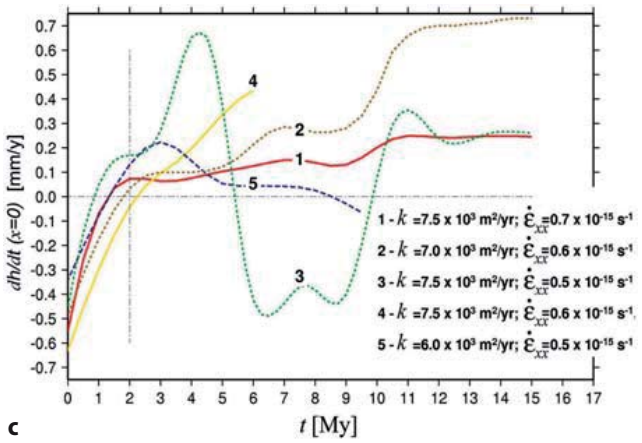

Fig. 5c. Tests of stability of the coupled "mountain growth" regime. Shown are the topography uplift rate at the axis ($x = 0$) of the range, for various deviations of the coefficient of erosion, k, and of the horizontal tectonic strain rates, $\partial\varepsilon_{xx}/\partial t$, from the values of the most stable reference case "1", which corresponds to the mountain growth experiment from Fig. 5b (bottom). Feedback between the surface and subsurface processes maintains the mountain growth regime even for large deviations of ks and $\partial\varepsilon_{xx}/\partial t$ (curves 2,3) from the equilibrium state (1). Cases 4 and 5 refer to very strong misbalance between the denudation and tectonic uplift rates, for which the system starts to collapse. These experiments suggest that the orogenic systems may be quite resistant to climatic changes or variations in tectonic rates, yet they rapidly collapse if the limits of the stability are exceeded

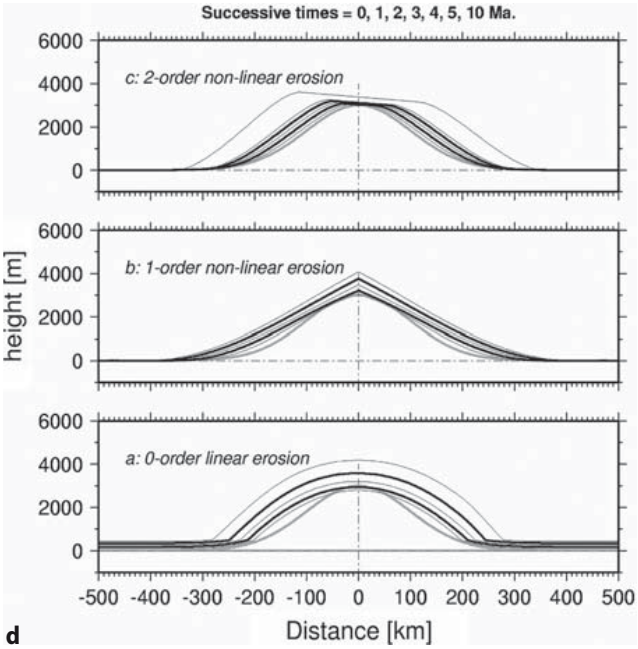

Fig. 5d. Influence of erosion law on steady-state topography shapes: 0 **a**, 1 **b**, and 2nd **c** order diffusion applied for the settings of the "mountain growth" experiment of Fig. 5b (bottom). The asymmetry in **c** arrives from smallwhite noise (1%) that was introduced in the initial topography to test the robustness of the final topographies. In case of highly non-linear erosion, the symmetry of the system is extremely sensitive even to small perturbations

6.1.4 Coupled Regime and Graded Geometries

In the coupled regime the topography of the range can be seen to develop into a nearly parabolic graded geometry (Fig. 5b). This graded form is attained after 2–3 My and reflects some dynamic equilibrium with the topographic rate of uplift being nearly constant over the range. Rates of denudation and of tectonic uplift can be seen to be also relatively constant over the range domain. Geometries for which the denudation rate is constant over the range are nearly parabolic since they are defined by

$$de/dt = k\,d^2h/dx^2 = \text{const.} \qquad (16)$$

Integration of this expression yields a parabolic expression for $h = x^2(de/dt)/2k + C_1x + C_0$, with C_1 and C_0 being constants to be defined from particular boundary conditions. The graded geometries obtained in the experiments slightly deviate from parabolic curves because they do not exactly correspond to uniform denudation over the range (h is also function of du/dt, etc.). This simple consideration does however suggest that the overall shape of graded geometries is primarily controlled by the erosion law. We then made computations assuming nonlinear diffusion laws, in order to test whether the setting of the coupled regime might depend on the erosion law. We considered nonlinear erosion laws, in which the increase of transport capacity downslope is modelled by a 1st order or 2nd order nonlinear diffusion (Eq. 4). For a given shortening rate, experiments that yield similar erosion rates over the range lead to the same evolution ("erosional collapse", "subsurface collapse", or "mountain growth") whatever is the erosion law. It thus appears that the emergence of the coupled regime does not depend on a particular erosion law but rather on the intensity of erosion relative to the effective viscosity of the lower crust. By contrast, the graded geometries obtained in the mountain growth regime strongly depend on the erosion law (Fig. 5d). The first order diffusion law leads to more realistic, than parabolic, "triangular" ranges whereas the 2nd order diffusion leads to plateau-like

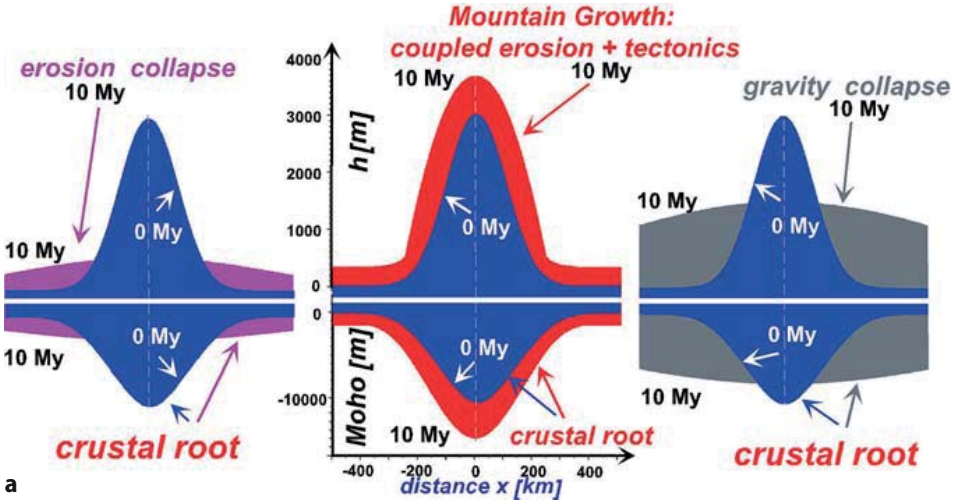

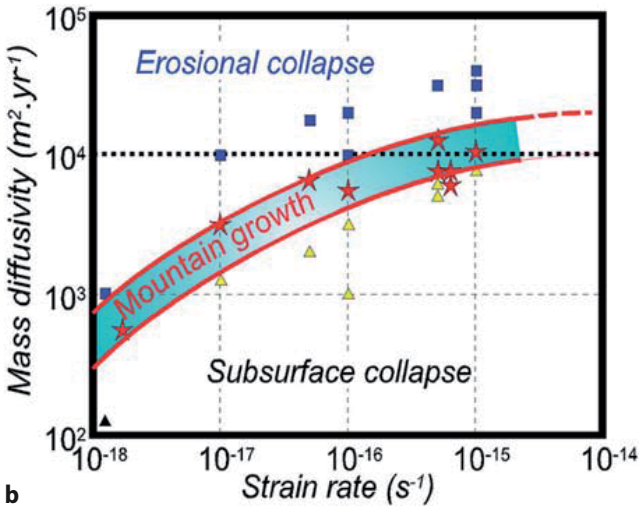

Fig. 6a. **a**) Summary of semi-analytical experiments: 3 major styles of topography evolution in terms of coupling between surface and sub-surface processes. **b**) Semi-analytical experiments: Modes of evolution of mountain ranges as a function of the coefficient of erosion (mass diffusivity) and tectonic strain rate, established for semi-analytical experiments with spatial resolution of 2 km x 2 km. Note that the coefficients of erosion are scale dependent, they may vary with varying resolution (or roughness) of the surface topography. Squares correspond to the experiments were erosional (surface) collapse was observed, triangles – experiments were subsurface collapse was observed, stars – experiments were localized stable growth of topography was observed

geometries. It appears that the graded geometry of a range may reflect the macroscopic characteristics of erosion. It might therefore be possible to infer empirical macroscopic laws of erosion from the topographic profiles across mountain belts provided that they are in a graded form.

6.1.5 Sensitivity to the Rheology and Structure of the Lower Crust

The above shown experiments have been conducted assuming a quartz rheology for the entire crust (= weak lower crust), which is particularly favorable for channel flow in the lower crust. We also conducted additional experiments assuming more basic lower crustal compositions (diabase, quartz-diorite). It appears that even with a relatively strong lower crust the coupled regime allowing for mountain growth can settle (Avouac and Burov, 1996). The effect of a less viscous lower crust is that the domain of values of the shortening rates and mass diffusivity for which the coupled regime can settle is simply shifted: at a given shortening rate lower rates of erosion are required to allow for the growth of the initial mountain. The domain defining the "mountain growth" regime in Fig. 6 is thus shifted towards smaller mass diffusivities when a stronger lower crust is considered. The graded shape obtained in this regime does not differ from that obtained with a quartz rheology. However, if the lower crust was strong enough to be fully coupled to the upper mantle, the dynamic equilibrium needed for mountain growth would not be established. Estimates of the yield strength of the lower crust near the Moho boundary for thermal ages from 0 to 2000 My. and for Moho depths from 0 to 80 km, made by Burov and Diament (1995), suggest that in most cases a crust thicker than about 40–50 km implies a low viscosity channel in the lower crust. However, if the lithosphere is very old or thin (> 1000 My), the coupled regime between erosion and horizontal flow in the lower crust will not develop.

6.1.6 Comparison with Observations

We compared our semi-analytical models with the Tien Shan range (Fig. 1a) because in this area, the rates of deformation and erosion have been well estimated from previous studies (Avouac et al., 1993: Metivier and Gaudemer, 1997), and because this range has a relatively simple 2-D geometry. The Tien Shan is the largest and most active mountain range in central Asia. It extends for nearly 2500 km between the Kyzil Kum and Gobi deserts, with some peaks rising to more than 7000 m. The high level of seismicity (Molnar and Deng, 1984) and deformation of Holocene alluvial formations (Avouac et al., 1993) would indicate a rate of shortening of the order of 1 cm/y. In fact, the shortening rate is thought to increase from a few mm/y east of 90°E to about 2 cm/y west of 76°E (Avouac et al., 1993). Clockwise rotation of the Tarim Basin (at the south of Tien Shan) with respect to Dzungaria and Kazakhstan (at the north) would be responsible for this westward increase of shortening rate as well as of the increase of the width of the range (Chen et al., 1991; Avouac et al., 1993). The gravity studies by Burov (1990) and Burov et al. (1990) also suggest westward decrease of the integrated strength of the lithosphere. The westward increase of the topographic load and strain rate could be responsible for this mechanical weakening. The geological record suggests a rather smooth morphology with no great elevation differences and low elevations in the Early Tertiary and that the range was reactivated in the middle Tertiary, probably as a result of the India-Asia collision (e.g., Tapponnier and Molnar, 1979; Molnar and Tapponnier, 1981; Hendrix et al., 1992; 1994). Fission track ages from detrital apatite from the northern and southern Tien Shan would place the reactivation at about 20 My (Hendrix et al., 1994; Sobel and Dumitru, 1995). Such an age is consistent with the middle Miocene influx of clastic material and more rapid subsidence in the forelands (Hendrix et al., 1992; Métivier and Gaudemer, 1997) and with a regional Oligocene unconformity (Windley et al., 1990). The present difference of elevation of about 3000 m between the range and the lowlands would therefore indicate a mean rate of uplift of the topography, during the Cenozoic orogeny, of the order of 0.1–0.2 mm/y. The foreland basins have collected most of the material removed by erosion in the mountain. Sedimentary isopachs indicate that $1.5\pm0.5 \times 10^6$ km^3 of material would have been eroded during the Cenozoic orogeny (Métivier and Gaudemer, 1997), implying erosion rates of 0.2–0.5 mm/y on average. The tectonic uplift would thus have been of 0.3–0.7 mm/y on average. On the assumption that the range is approximately in local isostatic equilibrium (Burov et al., 1990; Ma, 1987), crustal thickening below the range has absorbed 1.2 to 4 $\times 10^6$ km^3 (Métivier and Gaudemer, 1997). Crustal thickening would thus have accommodated 50 to 75% of the crustal shortening during the Cenozoic orogeny, with the remaining 25 to 50% having been fed back to the lowlands by surface processes. If we now place approximately the Tien Shan on the plot in Fig. 5 the 1 to 2 cm/y shortening corresponds to a basic strain rate of $\varepsilon_{xx} = 1.5–3 \times 10^{-16}$ s^{-1} and the 0.2–0.5 mm/y denudation rate implies a mass diffusivity of a few 10^3 to 10^4 m^2/y. These values actually place the Tien Shan in the "mountain growth" regime (Figs. 5b, 6). We therefore conclude that the localized growth of a range like the Tien Shan indeed could re-

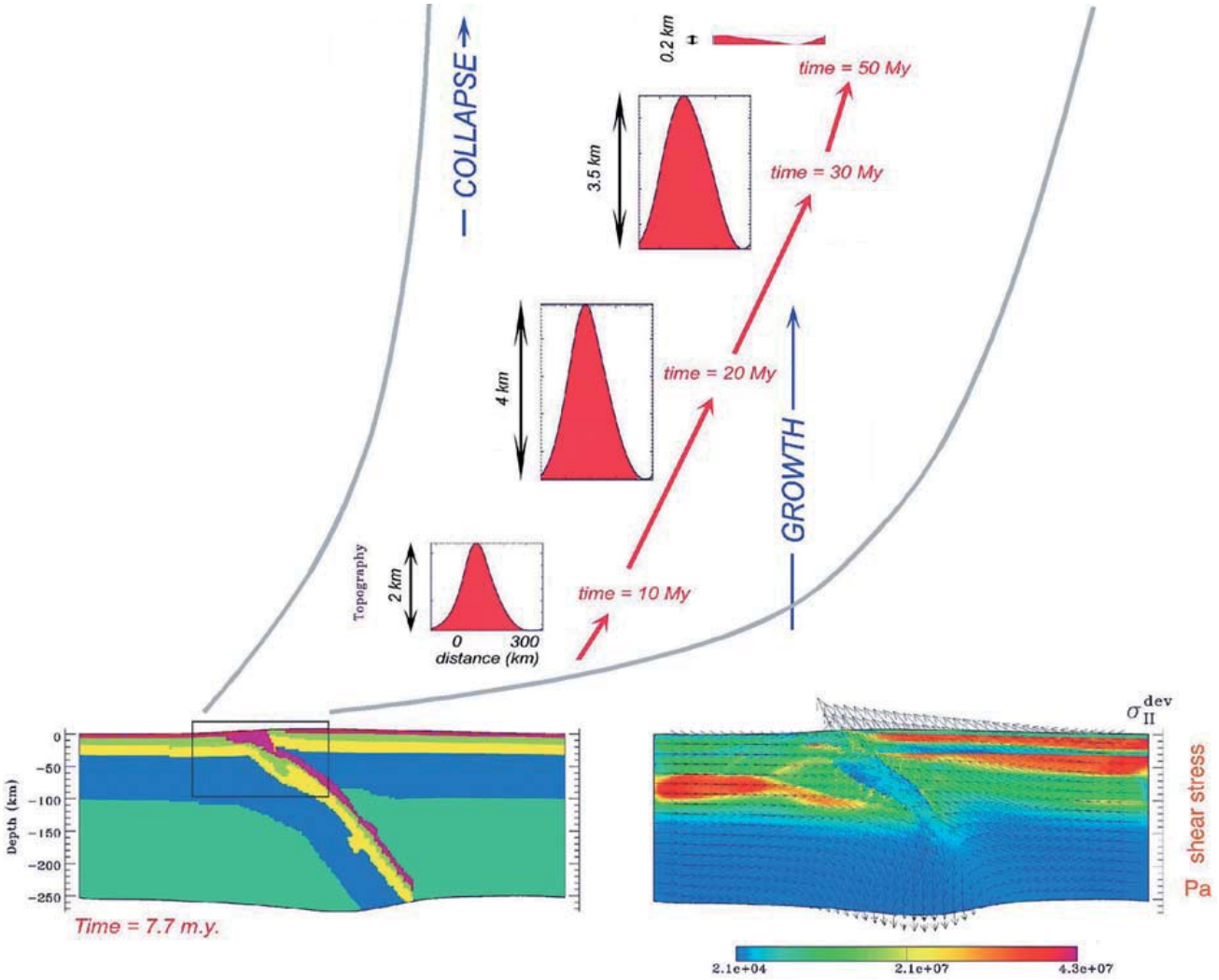

Fig. 7. Coupled numerical model of Alpine collision, with surface topography controlled by dynamic erosion. This model demonstrates that erosion-tectonics feedback help the mountain belt to remain as a localized growing feature for about 30 My. Note that final gravity collapse at 50 My results from erosion-tectonic misbalance after important amounts of shortening. Bottom, left: material phase field evolution at 7.7 My. Bottom, right: shear stress field. The numerical code (Parovoz) solves Newtonian force balance equations (large strain mode) coupled with brittle-ductile-elastic constitutive equations for main material phases, heat transfer equations and surface process equations. Colour code: purple – sediment/subduction channel; salad green – upper crust; yellow – lower crust; blue – lithosphere mantle; green – asthenosphere

sult from the coupling between surface processes and horizontal strains. We do not dispute the possibility for a complex mantle dynamics beneath the Tien Shan as has been inferred by various geophysical investigations (Vinnik and Saipbekova, 1984; Vinnik et al., 2006; Makeyeva et al., 1992; Roecker et al., 1993), but we contend that this mantle dynamics has not necessarily been the major driving mechanism of the Cenozoic Tien Shan orogeny.

6.2 Numerical Experiments

Fully numerical thermo-mechanical models were used to test more realistic scenarios of continental convergence (Fig. 4 bottom), in which one of the continental plates under-thrusts the other (simple shear mode, or continental "subduction"), the raising topography undergoes internal deformations, and the major thrust faults play an active role in localization of the deformation and in the evolution of the range. Also, in the numerical experiments, there is no pre-defined initial topography, which forms and evolves in time as a result of deformation and coupling between tectonic deformation and erosion processes. We show the tests for two contrasting cases: slow convergence and slow erosion (Western Alps, 6 mm/y, k = 500–1000 m^2/y) and very fast convergence and fast erosion (India - Himalaya collision, 6 cm/y during the first stage of continent-continent subduction, up to 15 cm/y at the preceding

stage of oceanic subduction, k = 3000–10000 m^2/y). The particular interest of testing the model for the conditions of the India-Himalaya-Tibet collision refers to the fact that this zone of both intensive convergence (Patriat and Achache, 1984) and erosion (e.g., Hurtrez et al., 1999) belongs to the same geodynamic framework of India-Eurasia collision as the Tien Shan range considered in the semi-analytical experiments discussed in the previous sections (Fig. 1a).

For the Alps, characterized by slow convergence and erosion rates (around 6 mm/y (Schmidt et al., 1997), k=500–1000 m^2/y according to Fig. 6), we have studied a scenario in which the lower plate has already subducted to a 100-km depth below the upper plate (Burov et al., 2001). This assumption was needed to enable the continental subduction since, in the Alps, low convergence rates make model initialization of the subduction process very difficult without a perfect knowledge of the initial configuration (Toussaint et al., 2004a). The numerical experiments (Fig. 7) confirm the idea that surface processes (k=500 m^2/y), which selectively remove the most rapidly growing topography, result in dynamic tectonically-coupled unloading of the lithosphere below the thrust belt, whereas the deposition of the eroded matter in the foreland basins results in additional subsidence. As a result, a strong feedback between tectonic and surface processes can be established and regulate the processes of mountain building during a very long period of time (in the experiments, 50 My): the erosion-sedimentation prevents the mountain from reaching gravitationally unstable geometries. The "Alpine" experiments demonstrate that the feedback between surface and tectonic processes may allow the mountains to survive over very large time spans (50 My). This feedback favors localized crustal shortening and stabilizes topography and

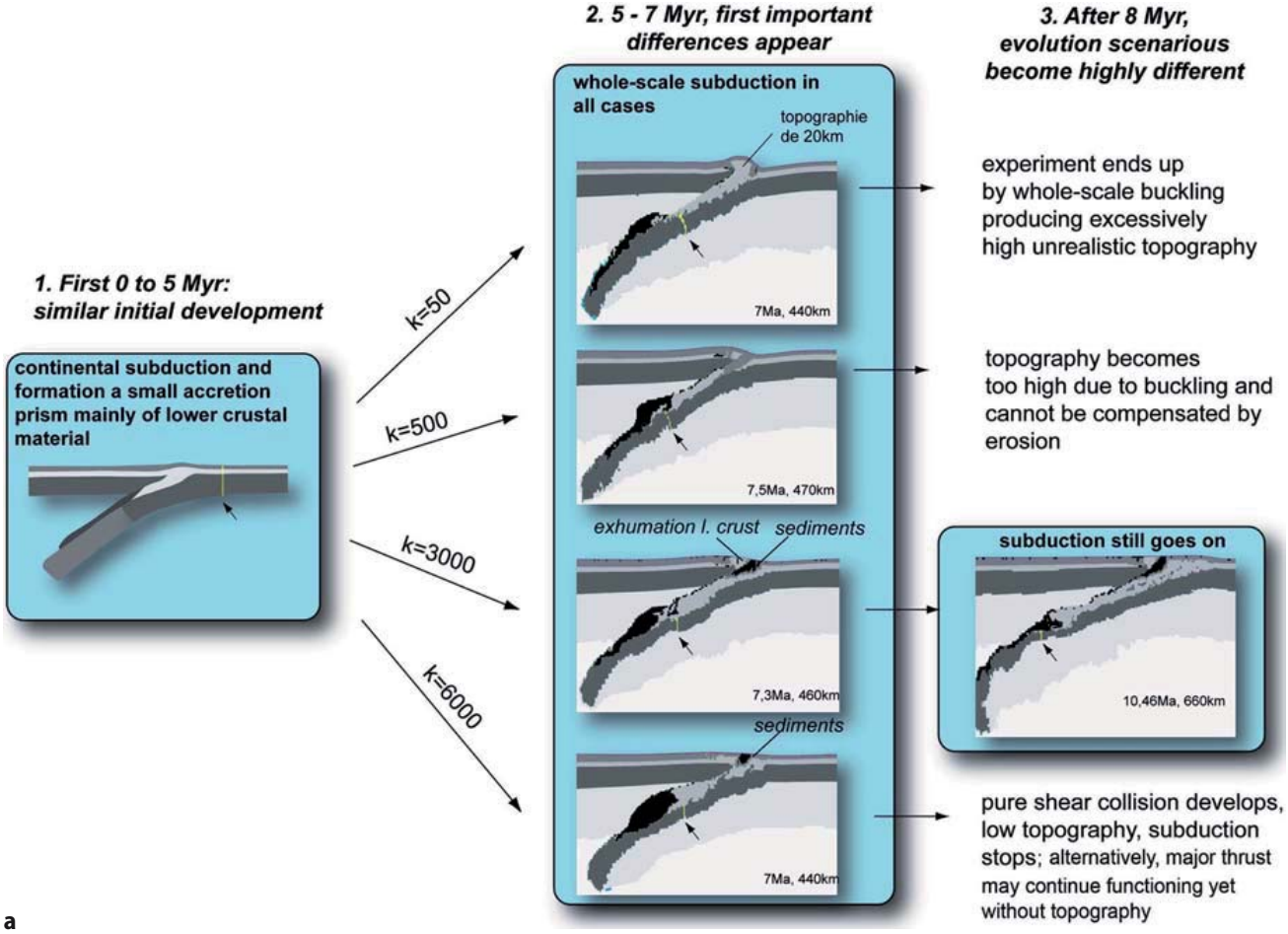

a

Fig. 8a. Coupled numerical models of India-Eurasia type of collision as function of the coefficient of erosion. These experiments were performed in collaboration with G. Toussaint using numerical setup (Fig. 4, bottom) identical to (Toussaint et al., 2004b). The numerical method is identical to that of (Burov et al., 2001 and Toussaint et al., 2004a,b; see also the experiment shown in Fig. 7). Sub-vertical stripes associated with little arrows point to the position of the passive marker initially positioned across the middle of the foreland basin. Displacement of this marker indicates the amount of subduction. Δx is amount of shortening. Different brittle-elastic-ductile rheologies are used for sediment, upper crust, lower crust, mantle lithosphere and the asthenosphere (Table 1b)

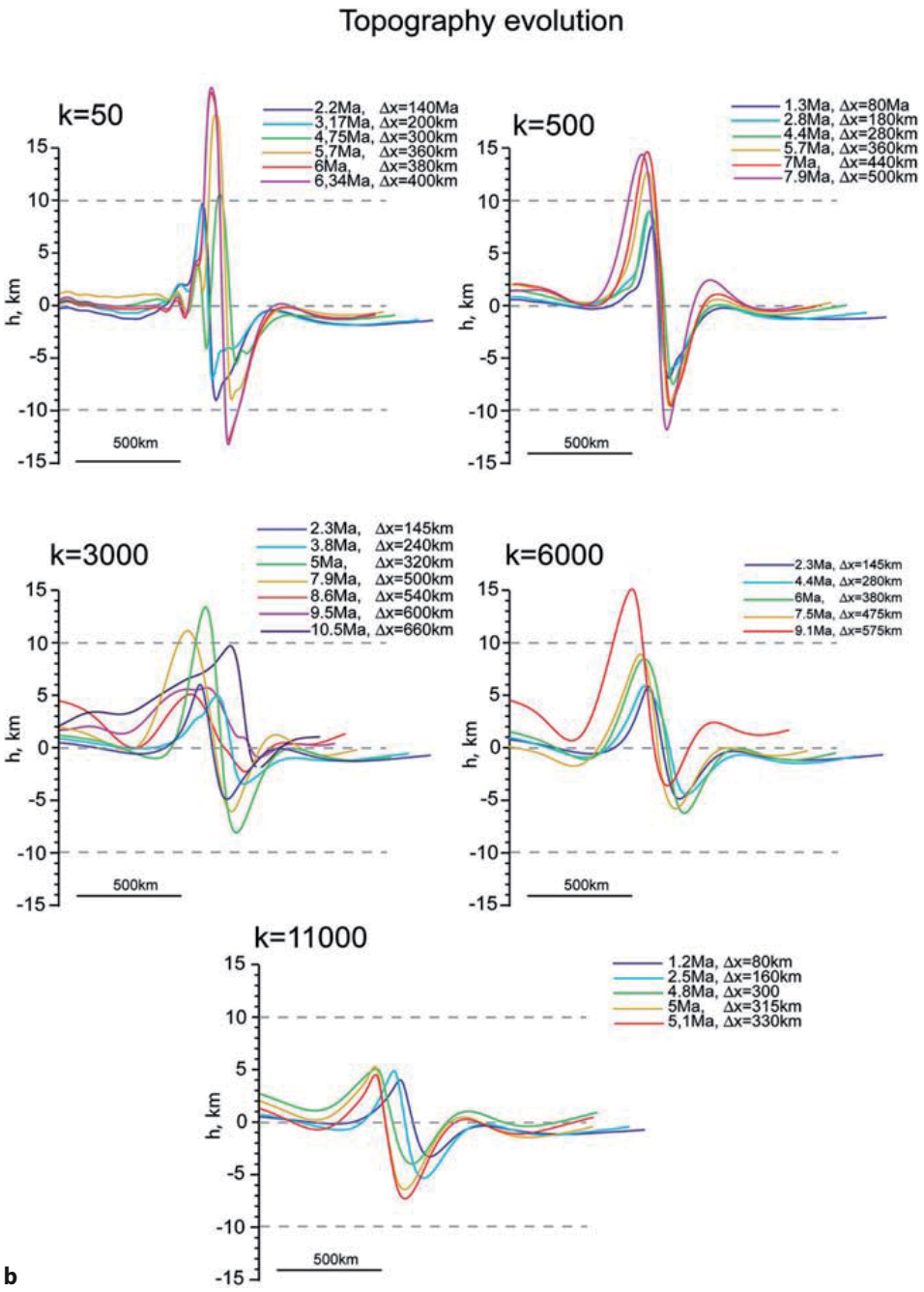

Fig. 8b. Smoothed surface profiles generated in the experiments of Fig. 8a (India-Eurasia type of collision). k is coefficient of erosion. Topography is unrealistically high for small $k = 50$ m^2/y , and too low for high $k > 1000$ m^2/y; the range 500 m^2/y $< k <$ 3000 m^2/y corresponds to localized mountain growth. Note complex behavior of the topography in case of $k = 3000$ m^2/y: The mountain range and the major thrust tend to migrate towards the subducting plate

thrust faults in time. Indeed even though a slow convergence scenario is not favorable for continental subduction, the model shows that once it is initialised, the tectonically coupled surface processes help to keep the major thrust working. Otherwise, in the absence of a strong feedback between surface and subsurface processes, the major thrust fault is soon blocked, the upper plate couples with the lower plate, and the system evolution turns from simple shear subduction to pure shear collision (Toussaint et al., 2004a; Cloetingh et al., 2004). However, topography cannot infinitely grow even in the "feedback" mode: as soon as the range grows to some critical size, it cannot be supported anymore due to the limited strength of the constituting rocks, and ends up by gravitational collapse. This has happened in the Alpine experiment towards 50 My of convergence (Fig. 7).

Our experiments on the fast "Indian-Asia" collision were based on the results of Toussaint et al. (2004b). The model and the entire setup (Figure 4, bottom) are identical to those described in detail in Toussaint et al. (2004b). For this reason, we refer the interested reader to this study (see also Appendix D and description of the numerical model in the previous sections). Toussaint et al. (2004b) tested the possibility of subduction of the Indian plate beneath the Himalaya and Tibet at

early stages of collision (first 15 My). This study used by default the "stable" values of the coefficient of erosion (3000±1000 m^2/y) derived from the semi-analytical model of (Avouac and Burov, 1996) for a shortening rate of 6 cm/y. The coefficient of erosion was only slightly varied in a way to keep the topography in reasonable limits, yet, Toussaint et al. (2004b) did not test the sensitivities of the Himalayan orogeny to large variations in the erosion rate. Our new experiments fill this gap by testing the stability of the same model for a large range of k, from 50 m^2/y to 11,000 m^2/y. These experiments (Fig. 8) demonstrate that, depending on the intensity of the surface processes, horizontal compression of continental lithosphere can lead either to strain localization below a growing range and continental subduction; or to distributed thickening or buckling/folding (Fig. 8a). The experiments suggest that homogeneous thickening occurs when erosion is either too strong (k > 1000 m^2/y), in that case any topographic irregularity is rapidly erased by surface processes (Fig. 8b), or when erosion is too weak (k < 50 m^2/y). In case of small k, surface elevations are unrealistically high (Fig. 8b), which leads to vertical over-loading and failure of the lithosphere and to an increase of the frictional force along the major thrust fault. As a consequence, the thrust fault is locked up leading to coupling between the upper and lower plate; this results in overall buckling of the region whereas the crustal root below the range starts to spread out laterally with formation of a flat "pancake-shaped" topography. On the contrary, in case of a dynamic balance between surface and subsurface processes (k = 2000 – 3000 m^2/y, close to the predictions of the semi-analytical model, Fig. 6), erosion/sedimentation resulted in long-term localization of the major thrust fault that kept active during 10 My. At the same time, in the experiments with k = 500–1000 m^2/y (moderate feedback between surface and subsurface processes), the major thrust fault and topography were almost stationary (Fig. 8a). In case of a stronger feedback (k = 2000–5000 m^2/y) the range and the thrust fault migrated horizontally in the direction of the lower plate ("India"). This basically happened when both the mountain range and the foreland basin reached some critical size. In this case, the "initial" range and major thrust fault were abandoned after about 500 km of subduction, and a new thrust fault, foreland basin and range were formed "to the south" (i.e., towards the subducting plate) of the initial location. The numerical experiments confirm our previous idea that intercontinental orogenies could arise from coupling between surface/climatic and tectonic processes, without specific help of other sources of strain localization. Given the differences in the problem setting, the results of the numerical experiments are in good agreement with the semi-analytical predictions (Fig. 6) that predict mountain growth for k on the order of 3000–10,000 m^2/y for strain rates on the order of 0.5×10^{-16} s^{-1}–10^{-15} s^{-1}. The numerical experiments, however, predict somewhat smaller values of k than the semi-analytical experiments. This can be explained by the difference in the convergence mode

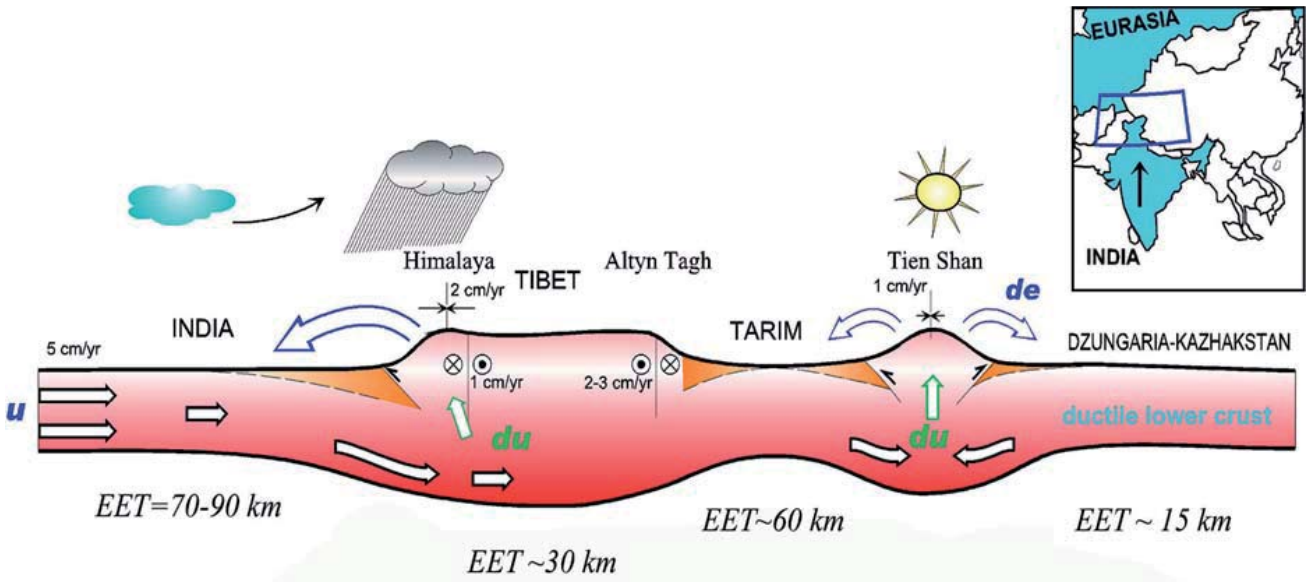

Fig. 9. Conceptual model for erosionally-controlled India - Eurasia collision derived from the numerical experiments. Asymmetry in climatic conditions to the south of the Himalaya with respect to Tibet to the north may explain the asymmetric development of the Himalayan-Tibetan region (Avouac and Burov, 1996). On the contrary, similar dry climatic conditions to the north and south of the Tien Shan range favour the development of its highly symmetric topography even if the colliding plates (Tarim block and Kazakh shield) have extremely contrasting mechanical properties (Burov et al., 1990; Vinnik et al., 2006)

attained in the numerical experiments (simple shear subduction) and in the analytical models (pure shear). For the same convergence rate, subduction resulted in smaller tectonic uplift rates than pure shear collision. Consequently, "stable" erosion rates and k values are smaller for subduction than for collision.

7 Conclusions

It appears that deformation of continents is highly sensitive to surface processes and, consequently, to climate. The surface processes may be a dominating factor of orogenic evolution that largely controls the evolution and shapes of the surface topography, major thrust faults, and foreland basins. For example, similar dry climatic conditions to the north and south of the Tien Shan range favor the development of its highly symmetric topography despite the fact that the colliding plates have extremely contrasting, asymmetric mechanical properties (in the Tarim block, the equivalent elastic thickness, EET = 60 km, whereas in the Kazakh shield, EET = 15 km (Burov et al., 1990)).

Although there is no perfect model for surface processes, the combination of modified diffusion and fluvial transport models provides satisfactory results for most large-scale tectonic applications.

In this study, we investigated the interactions between the surface and subsurface processes for three representative cases:

1. Very fast convergence rate, such as the India-Himalaya-Tibet collision.
2. Intermediate rate convergence settings (Tien Shan).
3. Very slow convergence settings (Western Alps).

In case of slow Alpine collision, we have shown that the persistence of once created topography may be insured by coupling between the surface and tectonic processes. Surface processes basically help to initialize and maintain continental subduction for a certain amount of time (5–7 My, maximum 10 My). They can stabilize, or "freeze" dynamic topography and the major thrust faults for as long as 50 My.

The way Central Asia has absorbed indentation of India may somehow reflect the sensitivity of the tectonic deformation to surface processes (Fig. 9) as asymmetry in climatic conditions to the south of the Himalaya with respect to Tibet to the north may explain the asymmetric development of the Himalaya-Tibetan region (Avouac and Burov, 1996). Interestingly, the mechanically asymmetric Tien Shan range situated north of Tibet, between the strong Tarim block and weak Kazakh shield, and characterized by similar climatic conditions at both sides of the range, is highly symmetric (Fig. 9). Previous numerical models of continental indentation that were based on continuum mechanics, but neglected surface processes, predicted a broad zone of crustal thickening, resulting from nearly homogeneous straining, that would propagate away from the indentor. In fact, crustal straining in Central Asia has been very heterogeneous and has proceeded very differently from the predictions of these models: a long-lived zone of localized crustal shortening has been maintained, in particular along the Himalaya, at the front of the indentor, and the Tien Shan, well north of the indentor; broad zones of thickened crust have resulted from sedimentation rather than from horizontal shortening (in particular in the Tarim basin, and to some extent in some Tibetan basins such as the Tsaïdam (Métivier and Gaudemer, 1997). Present kinematics of active deformation in Central Asia corroborates a highly heterogeneous distribution of strain. The 5cm/y convergence between India and stable Eurasia is absorbed by lateral extrusion of Tibet and crustal thickening, with crustal thickening accounting for about 3cm/y of shortening. About 2 cm/y would be absorbed in the Himalayas and 1cm/y in the Tien Shan. The indentation of India into Eurasia has thus induced localized strain below two relatively narrow zones of active orogenic processes while minor deformation has been distributed elsewhere. Our point is that, as in our numerical experiments, surface processes might be partly responsible for this highly heterogeneous distribution of deformation that has been maintained over several millions or tens of millions of years (Fig. 9). First active thrusting along the Himalaya and in the Tien Shan may have been sustained during most of the Cenozoic thanks to continuous erosion. Second, the broad zone of thickened crust in Central Asia has resulted in part from the redistribution of the sediments eroded from the localized growing reliefs. Moreover, it should be observed that the Tien Shan experiences a relatively arid intracontinental climate while the Himalayas is exposed to a very erosive monsoonal climate. This disparity may explain why the Himalaya absorbs twice as much horizontal shortening as the Tien Shan. In addition, the nearly equivalent climatic conditions on the northern and southern flanks of the Tien Shan might have favored the development of a nearly symmetrical range. By contrast the much more erosive climatic conditions on the southern than on the northern flank of the Himalaya may have favored the development of systematically south vergent structures. While the Indian upper crust would have been delaminated and brought to the surface of erosion by north dipping thrust faults, the Indian lower crust would have flowed below Tibet. Surface processes might therefore have facilitated injection of Indian lower crust below Tibet. This would explain crustal thickening of Tibet with minor hori-

zontal shortening in the upper crust, and minor sedimentation.

We thus suspect that climatic zonation in Asia has exerted some control on the spatial distribution of the intracontinental strain induced by the India-Asia collision. The interpretation of intracontinental deformation should not be thought of only in terms of boundary conditions induced by global plate kinematics but also in terms of global climate. Climate might therefore be considered as a forcing factor of continental tectonics.

To summarize, we suggest three major modes of evolution of thrust belts and adjacent forelands (Fig. 6):

1. Erosional collapse (erosion rates are higher than the tectonic uplift rates. Consequently, the topography cannot grow).
2. Localized persistent growth mode. Rigid feedback between the surface processes and tectonic uplift/subsidence that may favor continental subduction at initial stages of collision.
3. Gravity collapse (or "plateau mode", when erosion rates are insufficient to compensate tectonic uplift rates. This may produce a plateaux in case of high convergence rate).

It is noteworthy (Fig. 5c) that while in the "localized growth regime", the system has a very important reserve of stability and may readapt to eventual changes in tectonic or climatic conditions. However, if the limits of stability are exceeded, the system will collapse in very rapid, catastrophic manner.

We conclude that surface processes must be taken into account in the interpretation and modelling of long-term deformation of continental lithosphere. Conversely, the mechanical response of the lithosphere must be accounted for when large-scale topographic features are interpreted and modelled in terms of geomorphologic processes. The models of surface processes are most realistic if treated in two dimensions in a horizontal plane, while most of the current mechanical models are two dimensional in the vertical cross-section. Hence, at least for this reason, a next generation of 3D tectonically realistic thermomechanical models is needed to account for dynamic feedbacks between tectonic and surface processes. With that, new explanations of evolution of tectonically active systems and surface topography can be provided.

Acknowledgements

The author thanks the reviewers, D. Garcia-Castellanos and S. Cloetingh for very useful comments on the manuscript.

References

Ahnert, F., (1970) Functional relationships between denudation, relief and uplift in large mid-latitude drainage basins, Am. J. Sci., 268, 243–263.

Ashmore, P. E., (1982) Laboratory modelling of gravel braided stream morphology, Earth Surf. Processes Landforms, 7, 201–225.

Andrews, D. J., R.C. Bucknam, (1987)Fitting degradation of shoreline scarps by a nonlinear diffusion model, J. Geophys. Res., 92, 12857–12867.

Avouac, J.P., (1993) Analysis of scarp profiles: evaluation of errors in morphologic dating, J. Geophys. Res., 98, 6745-6754.

Avouac, J.-P., Tapponnier, P., Bai, M., You, H., G. Wang, Active thrusting and folding along the northern Tien Shan and late Cenozoic rotation of the Tarim relative to Dzungaria and Kazakhstan, J. Geophys. Res., 98, 6755–6804, 1993.

Avouac, J.-P., P. Tapponnier, (1993) Kinematic model of active deformation in Central Asia, Geophysical Research Letters, 20, 895–898.

Avouac, J. P., E. B. Burov, (1996) Erosion as a driving mechanism of intracontinental mountain growth, J. Geophys. Res., 101(B8), 17,747 –17,769.

Basile, C., P. Allemand, (2002) Erosion and flexural uplift along transform faults, Geophys. J. Int. 151, 646–653

Batchelor, G.K., (1967) An introduction to fluid dynamics, Cambridge University Press, p.615 Beaumont, C., (1981) Foreland basins, R. Astr. Soc. Geophys. J., 65, 389–416.

Beaumont, C., Fullsack, P., and J. Hamilton, Erosional control of active compressional orogens, Thrust Tectonics, Ed. K.R. McClay, Chapman & Hall, London, 1–31, 1992.

Beaumont, C., Fullsack, P., and J. Hamilton, Styles of crustal deformation in compressional orogens caused by subduction of the underlying lithosphere, submitted to: Proceedings of 5th International Symposium on Seismic Reflection Probing of the Continents and their Margins, eds.: R. Clowes and A. Green, 1994.

Beaumont, C., H. Kooi, and S. Willett, Coupled tectonic-surface process models with applications to rifted margins and collisional orogens, in Geomorphology and Global Tectonics, edited by M. A. Summerfield, pp. 29–55, John Wiley, New York, 2000.

Bonnet, S., and A. Crave, (2003) Landscape response to climate change: Insights from experimental modeling and implications for tectonic versus climatic uplift of topography, Geology, 31, 123–126.

Braun, J., and M. Sambridge, Modelling landscape evolution on geological time scales: A new method based on irregular spatial discretization, Basin Res., 9, 27– 52, 1997.

Beekman, F., (1994) Tectonic modelling of thick-skinned compressional intraplate deformation, PhD thesis, Free University, Amsterdam.

Bird, P., and A. J. Gratz, (1990) A theory for buckling of the mantle lithosphere and Moho during compressive detachments in continents, Tectonophysics, 177, 325–336.

Bird, P., (1991) Lateral extrusion of lower crust from under high topography in the isostatic limit, J. Geophys. Res., 96, 10275–10286.

Brace, W.F., and D.L. Kohlstedt, Limits on lithospheric stress imposed by laboratory experiments. J. Geophys. Res., 85, 6248–6252, 1980.

Byerlee, J. D., (1978) Friction of rocks. Pure Appl. Geophys., 116, 615–626.

Burbank, D.W., Causes of recent Himalayan uplift deduced from deposited patterns in the Ganges basin, Nature, 357, 680–683, 1992.

Burbank, D. W., and J. Vergés, (1994) Reconstruction of topography and related depositional systems during active thrusting, J. Geophys. Res., 99, 20,281–20,297.

Burov, E.V., M.G. Kogan, H. Lyon-Caen, and P. Molnar, Gravity anomalies, the deep structure, and dynamic processes beneath the Tien Shan, Earth Planet. Sci. Lett., 96, 367–383, 1990.

Burov, E. B., and Diament, (1992) M., Flexure of the continental lithosphere with multilayered rheology, Geophys. J. Int., 109, 449–468.

Burov, E. B., Lobkovsky, L.I., Cloetingh, S., and Nikishin, A. M., Continental lithosphere folding in Central Asia (part 2), constraints from gravity and topography, Tectonophysics, 226, 73–87, 1993.

Burov, E.B., and S. Cloetingh, (1997) Erosion and rift dynamics: new thermomechanical aspects of post-rift evolution of extensional basins, Earth and Planet Sci. Lett., 150, 7–26.

Burov, E.B. and M Diament, (1995) The effective elastic thickness (Te) of continental lithosphere: What does it really mean? J. Geophys. Res., 100, 3905–3927.

Burov, E.B., Jolivet, L., Le Pourhiet, L., and A. Poliakov, A thermemechanical model of exhumation of HP and UHP methamorphic rocks in Alpine mountain belts, Tectonophysics, 113–136, 2001.

Burov, E., A.B. Watts, The long-term strength of continental lithosphere: "jelly-sandwich" or "crème-brûlé"?, GSA Today, 16, 1, doi: 10.1130/1052–5173(2006)016<4:TLTSOC, 2006.

Carson, M.A., and M.J. Kirkby, (1972) Hillslope Form and Processes, Cambridge University Press, 475p.

Carter, N.L., and M.C. Tsenn, (1987) Flow properties of continental lithosphere, Tectonophysics, 36, 27–63.

Castelltort, S., and G. Simpson, (2006) Growing mountain ranges and quenched river networks, CRAS.

Chen, Y., Cogne, J.P., Courtillot, V., Avouac, J.P., Tapponnier, P., Buffetaut, E., Wang., G., Bai., M., You, H., Li, M., and C. Wei, Paleomagnetic study of Mesozoic continental sediments along the northern Tien Shan (China) and heterogeneous strain in Central Asia, J. Geophys. Res., 96, 4065–4082, 1991.

Chéry, J., Vilotte, J. P., and M. Daignieres, (1991) Thermomechanical evolution of a thinned continental lithosphere under compression: Implications for Pyrenees, J. Geophys. Res., 96, 4385–4412.

Chorley R.J., S.A. Schumm, and D.E. Sugden, (1984) Hillsopes in Geomorpholgy, 255–339, Methuen, London.

Cloetingh, S., Burov, E., Matenco L., Toussaint, G., and G. Bertotti, Thermo-mechanical constraints for the continental collision mode in the SE Carpathians (Romania), Earth and Planet Sci. Letters, 218(1–2), pp. 57–76, 2004.

Copeland P. and T.M. Harrison, (1990) Episodic rapid uplift in the Himalya revealed by 40Ar/39Ar analysis of detrital K-feldspar and muscovite, Bengal fan, Geology, 18, 354–357.

Crave, A., and P. Davy, A stochastic ''precipiton'' model for simulating erosion/sedimentation dynamics, Comput. Geosci., 27, 815– 827, 2001.

Crave, A., D. Lague, P. Davy, J. Kermarrec, D. Sokoutis, L. Bodet, and R. Compagnon, Analogue modelling of relief dynamics, Phys. Chem. Earth, Part A, 25(6–7), 549–553, 2000.

Culling, W.E.H., (1960) Analytical theory of erosion, Journal of Geology, 68, 336–333.

Culling, W.E.H., (1965) Theory of erosion on soil-covered slopes, Journal of Geology, 73, 230–254.

Cundall, P.A., (1989) Numerical experiments on localization in frictional material: Ingenieur-Archiv, v. 59, p. 148–159.

Davies, G. F., (1994) Thermomechanical erosion of the lithosphere by mantle plumes, J. Geophys. Res., 99, 15709–15722.

Davy, P., and A. Crave, (2000)Upscaling local-scale transport processes in largescale relief dynamics, Phys. Chem. Earth, Part A, 25(6–7), 533–541.

Densmore, A. L., R. S. Anderson, B. G. McAdoo, and M. A. Ellis, Hillslope evolution by bedrock landslides, Science, 275, 369– 372, 1997.

Densmore, A. L., M. A. Ellis, and R. S. Anderson, Landsliding and the evolution of normal fault-bounded mountain ranges, J. Geophys. Res., 103(B7), 15,203– 15,219, 1998.

Ellis, S., Fullsack, P., and C. Beaumont; Oblique convergence of the crust driven by basal forcing: implications for length-scales of deformation and strain partitioning in orogens, Geophys. J. Int., 120, 24–44, 1995.

England, P.C., and D.P. McKenzie, (1983) A thin viscous sheet model for continental deformation, Geophys. J. R. Astron. Soc., 73, 523–5323.

England, P., and S. W. Richardson, The influence of erosion upon the mineral facies of rocks from different metamorphic environments, J. Geol. Soc. Lond., 134, 201–213, 1977.

Flint, J. J., Experimental development of headward growth of channel networks, Geol. Soc. Am. Bull., 84, 1087– 1094, 1973.

Flint, J.-J., Stream gradient as a function of order magnitude, and discharge, Water Resour. Res., 10(5), 969–973, 1974.

Fleitout, L., and C. Froidevaux, Tectonics and topography for a lithosphere containing density heterogeneities, Tectonics, 1, 21–56, 1982.

Flemings, P. B., and T.E. Jordan, A synthetic stratigraphic model of foreland basin development, J. Geophys. Res., 94, 3851–3866, 1989.

Flemings, P. B., and T.E. Jordan, Stratigraphic modelling of foreland basins: interpreting thrust deformation and lithosphere rheology, Geology, 18, 430–434, 1990.

Fletcher, C.A.J., Computational techniques for fluid dynamics 2, Springer-Verlag, Berlin Heidelberg, 552 pp., 1988

Fournier, F., Climat et Erosion: la relation entre l'érosion du sol par l'eau et les précipitations atmosphériques, Presse Universitaire de France, Paris, 201 pp, 1960.

Gaspar-Escribano, J.M., Ter Voorde, M., Roca, E. and Cloetingh, S., Mechanical (de-)coupling of the lithosphere in the Valencia Through (NW Mediterranean): What does it mean ? Earth and Planet Sci. Lett., 210, 291–303, 2003

Garcia-Castellanos, D., Vergés, J., Gaspar-Escribano, J., and S. Cloetingh, Interplay between tectonics, climate, and fluvial transport during the Cenozoic evolution of the Ebro Basin (NE Iberia), J. Geophys. Res., VOL. 108, NO. B7, 2347, doi:10.1029/2002JB002073, 2003

Garcia-Castellanos, D., Interplay between lithospheric flexure and river transport in foreland basins, Basin Res., 14, 89–104, 2002.

Garcia-Castellanos, D., M. Fernàndez, and M. Torne, Modeling the evolution of the Guadalquivir foreland basin (southern Spain), Tectonics, 21(3), 1018, doi::10.1029/2001TC001339, 2002.

Gossman, H, Slope modelling with changing boundary conditions - effects of climate and lithology, Z. Geomoph. N.F., Suppl. Bd. 25, 72–88, 1976.

Govers, G., Evaluation of transporting capacity formulae for overland flow, in Overland Flow: Hydraulics and Erosion Mechanics, edited by A. J. Parsons and A. D. Abrahams, pp. 243 – 273, UCL Press, London, 1992a.

Govers, G., Relationship between discharge, velocity and flow area for rills eroding loose, non-layered materials, Earth Surf. Processes Landforms, 17, 515–528, 1992b.

Gratton, J., Crustal shortening, root spreading, isostasy, and the growth of orogenic belts: a dimensional analysis, J. Geophys. Res., 94, 15627-15634, 1989.

Gregory, K.M., and C. Chase, Tectonic and climatic significance of a late Eocene low-relief, high-level geomorphic surface, Colorado, J. Geophys. Res., 99, 20141–20160, 1994.

Hamilton, J.M, Kim, J., and F. Waleffe, Regeneration mechanisms of near-wall turbulence structures, J. Fluid. Mech., 287, 317–348, 1995.

Hanks, T.C., Buckham, R.C., LaJoie, K.R., and R.E. Wallace, Modification of wave-cut and fault-controlled landforms, J. Geophys. Res., 89, 5771-5790, 1984.

Hansen, E.B., and M.A. Kelmanson, An integral equation justification of the boundary conditions of the driven-cavity problem, Computers & Fluids, 23, 1, 225–240, 1994.

Hairsine, P. B., and C. W. Rose, Modeling water erosion due to overland flow using physical principles, 1, Sheet flow, Water Resour. Res., 28(1), 237–243, 1992.

Hancock, G., and G. Willgoose, Use of a landscape simulator in the validation of the SIBERIA catchment evolution model: Declining equilibrium landforms, Water Resour. Res., 37(7), 1981– 1992, 2001.

Hasbargen, L. E., and C. Paola, Landscape instability in an experimental drainage basin, Geology, 28(12), 1067– 1070, 2000.

Hendrix, M.S., Graham., S.A., Caroll, A.R., Sobel, E.R., McKnight, C.L., Schulein, B.J., and Z. Wang, Sedimentary record and climatic implications of recurrent deformation in the Tien Shan: Evidence from Mesozoic strata of the north Tarim, south Junggar, and Turpan basins, northwest China, Geol. Soc. of Am. Bull., 104, 53–79, 1992.

Hendrix, M.S., T.A., Dumitru and S.A; Graham, Late Oligocene-early Miocene unroofing in the Chinese Tian Shan: An early effect of the India Asia collision, Geology, 487–490, 1994.

Hirano, Simulation of developmental process of interfluvial slopes with reference to graded form, J. Geol, 83, 113–123, 1975.

Howard, A. D., Long profile development of bedrock channels: Interaction of weathering, mass wasting, bed erosion and sediment transport, in Rivers Over Rock: Fluvial Processes in Bedrock Channels, Geophys. Monogr. Ser., vol. 107, edited by K. J. Tinkler and E. E. Wohl, pp. 297– 319, AGU, Washington, D.C., 1998.

Howard, A. D., W. E. Dietrich, and M. A. Seidl, Modeling fluvial erosion on regional to continental scales, J. Geophys. Res., 99(B7), 13,971 – 13,986, 1994.

Huppert, H.E., The propagation of two dimensional and axisymmetric gravity currents over a rigid horizontal surface, J. Fluid. Mech., 121, 43–58, 1982.

Hurtrez, J.-E., F. Lucazeau, J. Lave´, and J.-P. Avouac, Investigation of the relationships between basin morphology, tectonic uplift, and denudation from the study of an active fold belt in the Siwalik Hills, central Nepal, J. Geophys. Res., 104(B6), 12,779– 12,796, 1999.

Kaufman, P.S., and L.H. Royden, Lower crustal flow in an extensional setting: Constraints from the Halloran Hills region, eastern Mojave Desert, California, J. Geophys. Res., 99, 15723–15739, 1994.

King, G.C.P., R.S. Stein a,d J.B. Rundle, The growth of geological structures by repeated earthquakes, 1. Conceptual framework, J. Geophys. Res., 93, 13307–13318, 1988.

King, G., and Ellis, The origin of large local uplift in extensional regions, Nature, 348, 689–693, 1990.

Kirby, S.H., Rheology of the lithosphere. Rev. Geophys., 21, 1458 –1487, 1983.

Kirby, S.H., and A.K. Kronenberg, Rheology of the lithosphere: Selected topics, Rev. of Geophys., 25, 1219–1244, 1987.

Kirkby, M. J., Hillslope process-response models based on the continuity equation, Spec. Publ. Inst. Br. Geogr., 3, 15– 30, 1971.

Kirkby, M.J. A two-dimensional model for slope and stream evolution, in Abrahams, A.D. ed., Hillslope Processes: Boston, Allen and Unwin., 203–224, 1986

Kirkby, M., Leeder, M., and N. White, The erosion of actively extending tilt-blocks: a coupled for topography and sediment budgets, application to the B&R, 13 pp., 1993.

Koch, D.M., and D. L. Koch, Numerical and theoretical solutions for a drop spreading below a free fluid surface, J. Fluid Mech., 287, 251–278, 1995.

Kohlstedt, D. L., Evans, B., and Mackwell; S. J., Strength of the lithosphere: Constraints imposed by laboratory experiments: Journal of Geophysical Research, 100, 17,587–17,602, 1995.

Kooi, H., and C. Beaumont, Escarpment evolution on high-elevation rifted margins: Insights derived from a surface processes model that combines diffusion, advection and reaction, J. Geophys. Res., 99, 12191–12209, 1994.

Kooi, H., and C. Beaumont, Large-scale geomorphology: Classical concepts reconciled and integrated with contemporary ideas via a surface processes model, J. Geophys. Res., 101(B2), 3361– 3386, 1996.

Kruse, S., M. McNutt, J. Phipps-Morgan, and L. Royden, Lithospheric extension near lake Mead, Nevada: A model for ductile flow in the lower crust, J. Geophys. Res., 96(3), 4435–4456, 1991.

Kusznir, N.J.; and D.H. Matthews, Deep seismic reflections and the deformational mechanics of the continental lithosphere, J. petrol., Spec. Lithosphere Issue, 63–87, 1988.

Kusznir, N.J., The distribution of stress with depth in the lithosphere: thermo-rheological and geodynamic constraints, Phil. Trans. R. Soc. Lond., A337, 95–110, 1991.

Lague, D., P. Davy, and A. Crave, Estimating uplift rate and erodibility from the area– slope relationship: Examples from Brittany (France) and numerical modelling, Phys. Chem. Earth, Part A, 25(6– 7), 543– 548, 2000.

Lague, D., A. Crave, and Ph. Davy, Laboratory experiments simulating the geomorphic response to tectonic uplift, J. Geophys. Res., VOL. 108, NO. B1, 2008, doi:10.1029/2002JB001785, 2003

Lavé, J., and J. P. Avouac, Fluvial incision and tectonic uplift across the

Himalayas of central Nepal, J. Geophys. Res., 106(B11), 26,561–26,591, 2001.

Leeder, M.R., Denudation, vertical crustal movements and sedimentary basin infill, Geologische Rundschau, Stuttgart, 80, 2, 441–458, 1991.

Le Pourhiet L, Burov E, Moretti I., Rifting through a stack of inhomogeneous thrusts (the dipping pie concept), Tectonics, 23 (4): TC4005, doi:10.1029/2003TC001584, 2004

Lobkovsky, L.I., Geodynamics of Spreading and Subduction zones, and the two-level plate tectonics, Nauka, Moscow, 251 pp., 1988.

Lobkovsky, L.I. and V.I. Kerchman, A two-level concept of plate tectonics: application to geodynamics. Tectonophysics, 199, 343–374, 1991.

Luke, J.C., Mathematical models for landform evolution, J. Geophys. Res., 77, 2460–2464, 1972.

Luke, J.C., Special Solutions for Nonlinear Erosion Problems, J. Geophys. Res., 79, 4035–4040, 1974.

Ma, X., Lithospheric dynamic Atlas of China, China Cartographic Publishing House, Beijing, China, 1987.

Makeyeva, L.I., L.P. Vinnik and S.W. Roecker, Shear-wave splitting and small scale convection in the continental upper mantle, Nature, 358, 144–147, 1992.

Masek, J. G., Isacks, B. L., and E. J. Fielding, Rift flank uplift in Tibet: Evidence for a viscous lower crust, Tectonics, 13, 659–667, 1994a.

Masek, J. G., Isacks, B. L., Gubbels, T.L., and E. J. Fielding, Erosion and tectonics at the margins of continental plateaus, J. Geophys. Res., 99, 13941–13956, 1994b.

Metivier, F., and Y. Gaudemer, Mass transfer between eastern Tien Shan and adjacent basins (centralAsia): constraints on regionaltectonics and topography, Geophys. J. Int., 128, 1–17, 1997.

Molnar, P., Climate change, flooding in arid environments, and erosion rates, Geology, 29(12), 1071– 1074, 2001.

Molnar, P. and Q. Deng, Faulting associated with large earthquakes and the average rate of deformation in central and eastern Asia, J. Geophys. Res., 89, 6203–6228, 1984

Molnar, P., and H. Lyon-Caen, Some simple physical aspects of the support, structure, and evolution of mountain belts, in: Processes in continental lithospheric deformation, Geol. Soc. Am. Spec., Rap. 218, 179–207, 1988

Molnar P., and Tapponnier, A possible dependence of the tectonic strength on the age of the crust in Asia, Earth Planet. Sci. Lett., 52, 107–114, 1981.

Molnar, P., and P. England, Late Cenozoic uplift of mountain ranges and global climate change: chicken or egg, Nature, 346, 29–34, 1990.

Mizutani, T., Laboratory experiment and digital simulation of multiple fillcut terrace formation, Geomorphology, 24, 353–361, 1998.

Nash, D.B., Morphologic dating of degraded normal fault scarps, J. Geol., 88, 353–360, 1980.

Newman, W.I., Nonlinear diffusion: Self-similarity and travelling-waves, PAGEOPH, 121, 3, 417–441, 1983.

Newman, W.I., and D.L. Turcotte, Cascade model for fluvial geomorphology, Geophys. J. Int., 100, 433–439, 1990.

Parson, B., and J. Sclater, An analysis of the variation of ocean floor bathymetry and heat flow with age, J. Geophys. Res., 93, 8051–8063, 1977.

Patriat, P., and J. Achache, India-Eurasia collision chronology has implications for crustal shortening and driving mechanism of plates, Nature, 311, 615–621, 1984.

Pelletier, J.D., Persistent drainage migration in a numerical landscape evolution model. Geophys. Res. Lett., 31, doi:10.1029/2004GL020802, 2004.

Persson, K.S., Garcia-Castellanos D., and D. Sokoutis , River transport effects on compressional belts: First results from an integrated analogue-numerical model, J. Geophys. Res., VOL. 109, B01409, doi:10.1029/2002JB002274, 2004

Pinet, P., and M. Souriau, Continental erosion and large-scale relief, Tectonics, 7, 3, 563–582, 1988.

Ranalli, G., Rheology of the Earth: Chapman & Hall, Sec. Edition., London, 413 pp, 1995.

Roecker, S.W., Sabitova, T.M., Vinnik, L.P., Burmakov, Y.A., Golvanov, M.I., Mamatkanova, R., and L. Minirova, Three dimensional elastic wave velocity structure of the western and central Tien Shan, J. Geophys., Res., 98, 15779–15795, 1993.

Roering, J. J., J. W. Kirchner, L. S. Sklar, and W. E. Dietrich, Hillslope evolution by nonlinear creep and landsliding: An experimental study, Geology, 29(2), 143– 146, 2001.

Schmid, S. M., Pffifner, O. A., Schönborg, G., Froitzheim, N., and Kissling, E., Integrated cross-sections and tectonic evolution of the Alps along the Eastern Traverse. In: Deep structures of the Swiss Alps, O. A. Pffifner, P. Lehner, P. Heitzmann, S. Mueller and A. Steck (Editors), Birkhäuser, Basel, pp. 289–304, 1997.

Schorghofer, N., and D. H. Rothman, Acausal relations between topographic slope and drainage area, Geophys. Res. Lett., 29(13), 1633, doi:10.1029/2002GL015144, 2002.

Schumm, S. A., M. P. Mosley, and W. E. Weaver, Experimental Fluvial Geomorphology, John Wiley, New York, 1987.

Seidl, M. A., and W. E. Dietrich, The problem of channel erosion into bedrock, Catena Suppl., 23, 101– 124, 1992.

Sheperd, R. G., and S. A. Schumm, Experimental study of river incision, Geol. Soc. Am. Bull., 85, 257– 268, 1974.

Simpson G., and F. Schlunegger, Topographic evolution and morphology of surfaces evolving in response to coupled fluvial and hillslope sediment transport, J. Geophys. Res., VOL. 108, NO. B6, 2300, doi:10.1029/2002JB002162, 2003

Sklar, L., and W. E. Dietrich, River longitudinal profiles and bedrock incision models: Stream power and the influence of sediment supply, in Rivers Over Rock: Fluvial Processes in Bedrock Channels, Geophys. Monogr. Ser., vol. 107, edited by K. J. Tinkler and E. E. Wohl, pp. 237–260, AGU, Washington, D.C., 1998.

Sklar, L. S., and W. E. Dietrich, Sediment and rock strength controls on river incision into bedrock, Geology, 29(12), 1087–1090, 2001.

Smith, C. E., Modeling high sinuosity meanders in a small flume, Geomorphology, 25, 19– 30, 1998.

Smith, T. R., and F. P. Bretherton, Stability and the conservation of mass in drainage basin evolution, Water Resour. Res., 8(6), 1506– 1529, 1972.

Snyder, N. P., Bedrock channel response to tectonic, climatic, and eustatic forcing, Ph.D thesis, Dep. of Earth, Atmos., and Planet. Sci., Mass. Inst. of Technol., Cambridge, Mass., 2001.

Snyder, N. P., K. X. Whipple, G. E. Tucker, and D. J. Merritts, Landscape response to tectonic forcing: DEM analysis of stream profiles in the Mendocino triple junction region, northern California, Geol. Soc. Am. Bull., 112, 1250– 1263, 2000.

Simpson, G., Role of river incision in enhancing deformation. Geology 32 (2004), 341–344.

Sobel E. and T. A. Dumitru, Exhumation of the margins of the western Tarim basin during the Himalayan orogeny, Tectonics, in press, 1995

Stein, R.S., G.C.P. King and J.B. Rundle, The growth of geological structures by repeated earthquakes, 2. Field examples of

continental dip-slip faults, J. Geophys. Res., 93, 13319–13331, 1988.
Summerfield, M.A. and N.J. Hulton, Natural control on fluvial denudation rates in major world drainage basins, J. Geophys. Res., 99, 13871–13883, 1994.
Talbot, C.J., and R.J. Jarvis, Age, budget and dynamics of an active salt extrusion in Iran, J. Struct. Geology, 6, 521–533, 1984.
Tapponnier, P., and P. Molnar, Active faulting and Cenozoic tectonics of the Tien Shan, Mongolia and Baykal regions, J. Geophys. Res., 84, 3425–3459, 1979.
Ter Voorde, M., Van Balen, R.T., Bertotti, G. and Cloetingh, S.A.P.L., The influence of a stratified rheology on the flexural response of the lithosphere to (un)loading by extensional faulting. Geophys. J. Int., 134, 721–735, 1998.
Toussaint, G., Burov, E., and L. Jolivet, Continental plate collision: unstable versus stable slab dynamics, Geology, 32, No. 1, 33–36, 2004a.
Toussaint G., Burov, E., and J.-P. Avouac, Tectonic evolution of a continental collision zone: a thermo mechanical numerical model, Tectonics, 23, TC6003, doi:10.1029/2003TC001604, 2004b.
Tsenn, M.C. , and N.L. Carter, Flow properties of continental lithosphere. Tectonophysics, 136, 27–63, 1987.
Tucker, G. E., and R. L. Bras, Hillslope processes, drainage density, and landscape morphology, Water Resour. Res., 34(10), 2751– 2764, 1998.
Tucker, G. E., and R. L. Bras, A stochastic approach to modeling the role of rainfall variability in drainage basin evolution, Water Resour. Res., 36(7), 1953– 1964, 2000
Turcotte, D.L., and G. Schubert, Geodynamics. Applications of continuum physics to geological problems, J. Wiley & Sons, New York, 450 p., 1982.
Vinnik, L.P. and A.M. Saipbekova, Structure of the lithosphere and asthenosphere of the Tien Shan, Annales Geophysicae, 621–626, 1984.
Vinnik, L.P., I. M. Aleshin, M. K. Kaban, S. G. Kiselev, G. L. Kosarev, S. I. Oreshin, and Ch. Reigber, Crust and Mantle of the Tien Shan from Data of the Receiver Function Tomography, Izvestiya, Physics of the Solid Earth, 42, pp. 639–651, Pleiades Publishing, Inc., 2006.
Vilotte, J.P., M. Daignières and R. Madariaga, Numerical modeling of intraplate deformation: simple mechanical models of continental collision, J. Geophys. Res., 87, 10709–10728, 1982.
Vogt, P.R., Bermuda and Applachian-Labrador rises, common hotspot processes, Geology, 19, 41–44, 1991.
Wang J.N., B.E. Hobbs, A.Ord, T. Shimamoto, and M. Toriumi, Newtonian dislocation creep in quartzites: Implications for the rheology of the lower crust, Science, 265, 1204–1206,
Westaway, R., Evidence for dynamic coupling of surface processes with isostatic compensation in the lower crust during active extension of western Turkey, J. Geophys. Res., 99, 20203–20223, 1994.
Willett, S. D., Orogeny and orography: The effects of erosion on the structure of mountain belts, J. Geophys. Res., 104(B12), 28,957 – 28,982, 1999.
Windley, B. F., M.B. Allen, C., Zhang, Z.Y., Zhao, and G.R. Wang, Paleozoic accretion and Cenozoic redeformation of the Chinese Tien Shan range, central Asia, Geology, 18, 128–131, 1990.

Appendix A
Model of Flexural Deformation of the Competent Cores of the Brittle-Elasto-Ductile Crust and Upper Mantle

The vertical displacements of the competent layers in the crust and mantle in response to redistribution of surface and subsurface loads (Fig. 4, top) can be described by plate equilibrium equations in assumption of nonlinear rheology (Burov and Diament, 1995). We assume that the reaction of the competent layers is instantaneous (response time $dt \sim \mu_{min}/E < 10^3$ years, where μ_{min} is the minimum of effective viscosities of the lower crust and asthenosphere)

$$\frac{\partial}{\partial x}\left(\frac{\partial}{\partial x}\left(\frac{E}{12(1-\nu^2)}\,\widetilde{T}_e^3(\phi)\,\frac{\partial^2 w(x,t)}{\partial x^2}\right)+\widetilde{T}_x(\phi)\,\frac{\partial w(x,t)}{\partial x}\right)+p_-(\phi)\,w(x,t)-p_+(x,t)=0$$

$$\widetilde{T}_e(\phi)=\left(\frac{\widetilde{M}_x(\phi)}{L}\left(\frac{\partial^2 w(x,t)}{\partial x^2}\right)^{-1}\right)^{1/3}$$

$$\widetilde{M}_x(\phi)=-\sum_{i=1}^{n}\sum_{j=1}^{m_i}\int_{y_{ij}^-(\phi)}^{y_{ij}^+(\phi)}\sigma_{xx}^{(j)}(\phi)\,y_i^*(\phi)\,dy \qquad \text{(A.1)}$$

$$\widetilde{T}_x(\phi)=-\sum_{i=1}^{n}\sum_{j=1}^{m_i}\int_{y_{ij}^-(\phi)}^{y_{ij}^+(\phi)}\sigma_{xx}^{(j)}(\phi)\,dy$$

$$\sigma_{xx}^{(j)}(\phi)=sign(\varepsilon_{xx})\,\mathbf{min}\left(|\sigma^f|,\,\sigma_{xx}^{e(j)}(\phi)\right)$$

$$\sigma_{xx}^{e(j)}(\phi)=y_i^*(\phi)\,\frac{\partial^2 w(x,t)}{\partial x^2}\,E_i(1-\nu_i^2)^{-1}$$

where $w = w(x,t)$ is the vertical plate deflection (related to the regional isostatic contribution to tectonic uplift du_{is} as $du_{is} = w(x,t) - w(x,t-dt)$), $\phi \equiv \{x,y,w,w',w'',t\}$, y is downward positive, $y_i^* = y - y_{ni}(x)$, y_{ni} is the depth to the i^{th} neutral (i.e., stress-free, $\sigma_{xx}|_{y_i^*=0}$) plane; $y_i^-(x) = y_i^-$, $y_i^+(x) = y_i^+$ are the respective depths to the lower and upper low-strength interfaces (see Fig. A). σ^f is defined from Eqs. (10–11). n is the number of mechanically decoupled competent layers; m_i is the number of "welded" (continuous σ_{xx}) sub-layers in the ith detached layer. p_-w is a restoring stress ($p_- \sim (\rho_m - \rho_{c_1})g$) and p^+ is a sum of surface and subsurface loads. The most important contribution to p^+ is from the load of topography, that is, $p^+ \sim \rho g h(x,t)$, where the topographic height $h(x,t)$ is defined as $h(x,t) = h(x,t-dt) + dh(x,t) = h(x,t-dt) + du(x,t) - de(x,t)$, where $du(x,t)$ and $de(x,t)$ are, respectively tectonic uplift/subsidence and denu-

dation/sedimentation at time interval (t–dt, t), counted from sea level. The thickness of the ith competent layer is $y_i^+ - y_i^- = \Delta h_i(x)$. The term w" in (A.1) is inversely proportional to the radius of plate curvature $R_{xy} \approx -(w")^{-1}$. Thus, the higher is the local curvature of the plate, the lower is the local integrated strength of the lithosphere. The integrals in (A.1) are defined through the constitutive laws (6–9) and Eq. (10–11) relating the stress σ_{xx} and strain $\varepsilon_{xx} = \varepsilon_{xx}(\phi)$ in a given segment {x,y} of plate. The value of the unknown function $\tilde{T}_e(\phi)$ has a meaning of a "momentary" effective elastic thickness of the plate. It holds only for the given solution for plate deflection w. $\tilde{T}_e(\phi)$ varies with changes in plate geometry and boundary conditions. The effective integrated strength of the lithosphere (or $T_e = \tilde{T}_e(\phi)$) and the state of its interiors (brittle, elastic or ductile) depends on differential stresses caused by local deformation, while stresses at each level are constrained by the YSE. The nonlinear Eqs. (A.1) are solved using an iterative approach based on finite difference approximation (block matrix presentation) with linearization by Newton's method [Burov and Diament, 1992]. The procedure starts from calculation of elastic prediction $w_e(x)$ for $w(x)$, that provides predicted $w_e(x)$, $w_e'(x)$, $w_e"$ used to find subiteratively solutions for $y_{ij}^-(\phi)$, $y_{ij}^+(\phi)$, and $y_{ni}(\phi)$ that satisfy Eqs. (5), (6), (7), (10). This yields corrected solutions for $\tilde{M}_x$ and $\tilde{T}_x$ which are used to obtain $\tilde{T}_e$ for the next iteration. At this stage we use gradual loading technique to avoid numerical oscillations. The accuracy is checked directly on each iteration, through back-substitution of the current solution to Eq. (A.1) and calculation of the discrepancy between the right and left sides of Eq. (A.1). For the boundary conditions on the ends of the plate we use commonly inferred combination of plate-boundary shearing force $Q_x(0)$,

$$\tilde{Q}_x(\phi) = -\sum_{i=1}^{n}\sum_{j=1}^{m_i}\int_{y_{ij}^-(\phi)}^{y_{ij}^+(\phi)}\sigma_{xy}^{(j)}(\phi)dy \qquad (A.2)$$

and plate boundary moment $M_x(0)$ (in the case of broken plate) and $w = 0$, $w' = 0$ (and $h = 0$, $\partial h/\partial x = 0$) at $x \to \pm\infty$. The starting temperature distribution and yield-stress profiles (see above) are obtained from the solution of the heat transfer problem for the continental lithosphere of Paleozoic thermotectonic age, with average Moho thickness of 50 km, quartz-controlled crust and olivine-controlled upper mantle, assuming typical horizontal strain rates of $\sim 0.1 \div 10 \times 10^{-15}$ s^{-1}. (Burov et al., 1993; 1995). These parameters roughly resemble the Tien Shan and Tarim basin (Fig. 1a).

Burov and Diament (1995) have shown that the flexure of the continental lithosphere older than 200–250 My is predominantly controlled by the mechanical portion of mantle lithosphere (depth interval between T_c and h_2). Therefore, we associate the deflection of Moho with the deflection of the entire lithosphere (analogously to Lobkovsky and Kerchman, 1991; Kaufman and Royden, 1994; Ellis et al., 1995). Indeed, the effective elastic thickness of the lithosphere (T_e) is approximately equal to $\sqrt[3]{T_{ec}^3 + T_{em}^3}$, where T_{ec} is the effective elastic thickness of the crust and T_{em} is the effective elastic thickness of the mantle lithosphere (e.g., Burov and Diament, 1995). $\lim \sqrt[3]{T_{ec}^3 + T_{em}^3} \approx \max(T_{ec}, T_{em})$. T_{ec} cannot exceed h_{c1}, that is 15–20 km (in practice, $T_{ec} \leq$ 5–10 km). T_{em} cannot exceed h_2–$T_c \sim$ 60–70 km. Therefore $T_e \approx T_{em}$ which implies that total plate deflection is controlled by the mechanical portion of the mantle lithosphere.

Appendix B
Model of Flow in the Ductile Crust

As it was already mentioned, our model of flow in the low viscosity parts of the crust is similar to that formulated by Lobkovsky (1988), Lobkovsky and Kerchman (1991) (hereafter referred as L&K), or Bird (1991). However, our formulation can allow computation of different types of flow ("symmetrical", Poiseuille, Couette) in the lower crust (L&K considered Couette flow only). In the numerical experiments shown in this paper we will only consider cases with a mixed Couette/Poiseuille/symmetrical flow, but we first tested the same formulation as L&K. The other important difference with L&K's models is, naturally, the use of realistic erosion laws to simulate redistribution of surface loads, and of the realistic brittle-elastic-ductile rheology for modeling the response of the competent layers in the lithosphere.

Tectonic uplift $du(x,t)$ due to accumulation of the material transported through ductile portions of the lower and upper crust ($dh(x,t) = du(x,t) - de(x,t)$) can be modelled by equations which describe evolution of a thin subhorizontal layer of a viscous medium (of density ρ_{c2} for the lower crust) that overlies a non-extensible pliable basement supported by Winkler forces (i.e., flexural response of the mantle lithosphere which is, in-turn, supported by hydrostatic reaction of the astenosphere) (Batchelor, 1967; Kusznir and Matthews, 1988; Bird and Gratz, 1990; Lobkovsky and Kerchman, 1991; Kaufman and Royden, 1994).

The normal load, which is the weight of the topography $p_+(x)$ and of the upper crustal layer (thickness h_{c1} and density ρ_{c1}) is applied to the surface of the lower crustal layer through the flexible competent upper crustal layer. This internal ductile crustal layer of variable thickness $\Delta h_{c2} = \Delta h_0(x,0) + \tilde{h}(x) + w(x)$ is regionally compensated by the strength of the underlying competent mantle lithosphere (with density ρ_m).

Variation of the elevation of the upper boundary of the ductile layer ($d\tilde{h}$) with respect to the initial thickness ($\Delta h_0(x,0)$) leads to variation of the normal load applied to the mantle lithosphere. The regional isostatic response of the mantle lithosphere results in deflection (w) of the lower boundary of the lower crustal layer, that is the Moho boundary, which depth is $h_c(x,t) = T_c(x,t)=\Delta h_{c_2}+y_{13}$ (see Table 1a). The vertical deflection w (Eq. A.1) of the Moho depends also on vertical undulation of the elastic-to-ductile crust interface y_{13}.

The absolute value of $\tilde{h}$ is not equal to that of the topographic undulation h by two reasons: first, h is effected by erosion; second, $\tilde{h}$ depends not only on the uplift of the upper boundary of the channel, but also on variation of the thickness of the competent crust given by value of $y_{13}(x)$. We can require $\tilde{h}(x,t)-\tilde{h}(x,t-dt) = du-dy_{13}$. Here $dy_{13} = y_{13}(\phi,t)-y_{13}(\phi, t-dt)$ is the relative variation in the position of the lower boundary of the elastic core of the upper crust due to local changes in the level of differential (or deviatoric) stress (Fig. 5a). This flexure- and flow-driven differential stress can weaken material and, in this sense, "erode" the bottom of the strong upper crust. The topographic elevation $h(x,t)$ can be defined as $h(x,t) = h(x,t-dt)+d\tilde{h} -de(t)-dy_{13}$ where dy_{13} would have a meaning of "subsurface or thermomechanical erosion" of the crustal root by local stress.

The equations governing the creeping flow of an incompressible fluid, in Cartesian coordinates, are:

$$-\frac{\partial\sigma_{xx}}{\partial x}+\frac{\partial\tau_{xy}}{\partial y}+F_x=0;\ -\frac{\partial\sigma_{yy}}{\partial y}+\frac{\partial\tau_{xy}}{\partial x}+F_y=0$$

$$\sigma_{xx}=-\tau_{xx}+p=-2\mu\frac{\partial u}{\partial x}+p$$

$$\sigma_{xy}=\tau_{xy}=\mu\left(\frac{\partial u}{\partial y}+\frac{\partial v}{\partial x}\right) \qquad \text{(B.1a)}$$

$$\sigma_{yy}=-\tau_{yy}+p=-2\mu\ \frac{\partial v}{\partial x}+p$$

$$\frac{\partial u}{\partial x}+\frac{\partial v}{\partial y}=0 \qquad \text{(B.1b)}$$

$$\mu=\frac{\sigma}{2\dot{\varepsilon}}$$

$$\dot{\varepsilon}=\sigma^n A^* \exp(-H^*/RT) \qquad \text{(B.1c)}$$

where μ is the effective viscosity, p is pressure, u and v are the horizontal and vertical components of the velocity $\boldsymbol{v}$, respectively. F is the body force. $u = \partial\psi/\partial x$ is the horizontal component of velocity of the differential movement in the ductile crust, $v = -\partial\psi/\partial x$ is its vertical component; and $\partial u/dy = \dot{\varepsilon}_{c_{20}}$ is a component of shear strain rate due to the differential movement of the material in the ductile crust (the components of the strain rate tensor are consequently: $\dot{\varepsilon}_{11} = 2\partial u/dx$; $\dot{\varepsilon}_{12} = \partial u/dy+\partial v/dx$; $\dot{\varepsilon}_{22} = 2\partial v/dy$).

Within the low viscosity boundary layer of the lower crust, the dominant basic process is simple shear on horizontal planes, so the principal stress axes are dipped approximately $\pi/2$ from x and y (hence, σ_{yy} and σ_{xx} are approximately equal). Then, the horizontal component of quasi-static stress equilibrium equation $div\boldsymbol{\sigma}+\rho g = 0$, where tensor $\boldsymbol{\sigma}$ is $\boldsymbol{\sigma} = \boldsymbol{\tau}-P\mathbf{I}$ ($\mathbf{I}$ is identity matrix), can be locally simplified yielding thin layer approximation (e.g., Lobkovsky, 1988; Bird and Gratz, 1990):

$$\frac{\partial\tau_{xy}}{\partial y}=\frac{\partial p}{\partial x}-F_x=-\frac{\partial\tau_{yy}}{\partial x} \qquad \text{B.2)}$$

A basic effective shear strain-rate can be evaluated as $\dot{\varepsilon}_{xy} = \sigma_{xy}/2\mu_{eff}$, therefore, according to the assumed constitutive relations, horizontal velocity u in the lower crust is:

$$u(\tilde{y})=\int_0^{\tilde{y}}2\dot{\varepsilon}_{xy}\partial\tilde{y}+C_1= \\ =\int_0^{\tilde{y}}2^n A^*\exp(-H^*/RT(y))\left|\tau_{xy}\right|^{n-1}\tau_{xy}\,\partial\tilde{y}+C_1 \qquad \text{(B.3)}$$

Here $\tilde{y} = y-y_{13}$. $y_{13}=y_{13}(\phi)$ is the upper surface of the channel defined from solution of the system (A.1). C_1 is a constant of integration defined from the velocity boundary conditions. τ_{xy} is defined from vertical integration of Eq. (B.2). The remote conditions $h = 0$, $\partial h/\partial x = 0$, $w = 0$, $\partial w/\partial x = 0$ for the strong layers of the lithosphere (Appendix A) are in accordance with the condition for ductile flow: at $x \to \infty$ $u^+_{c_2} = u_c$; $u^-_{c_2} = u_m$; $\partial p/\partial x = 0$, $\partial p/\partial y = \bar{\rho}_c g$; $p = P_0$.

There is also an "inherent" boundary condition, free flow on the far ends of the ductile channel. From the formal point of view, the conservation of mass in the channel is not observed under this condition. However, it is not crucial in the particular case because the channel is long and has flexible walls (in the experiments, 30–50 times longer than its thickness and 10 times longer than total horizontal shortening). Therefore, local perturbations in the flow beneath the mount and basins do not reach the remote end(s) of the channel. In a general case, it is even reasonable to assume that the horizontal tectonic deformation on the ends of the plate is transmitted through the strong parts of the crust, while the low viscosity crust may flow in- or out of the system. In the particular numerical experiments described here, we checked the balance of volume and found the loss of mass to be negligible (< 5% of the entered volume).

In the trans-current channel flow the major perturbation to the stress (pressure) gradients is caused by slopes of crustal interfaces $\alpha \sim \partial\tilde{h}/\partial x$ and $\beta \sim \partial w/\partial x$. These slopes are controlled by flexure, isostatic re-adjustments, surface erosion, and by "erosion" (weakening) of the interfaces by stress and temperature. The later especially concerns the upper crustal interface. In the assumption of small plate defections, the horizontal force associated with variation of the gravitational potential energy due to deflection of Moho (w) is $\rho_{c_2} g \tan(\beta) \sim \rho_{c_2} g \sin(\beta) \sim \rho_{c_2} g \partial w/\partial x$; the vertical component of force is respectively $\sim\rho_{c_2} g \cos(\beta) \sim \rho_{c_2} g (1-\partial w/\partial x) \sim \rho_{c_2} g$. The horizontal and vertical force components due to slopes of the upper walls of the channel are respectively $\rho_{c_2} g \tan(\alpha) \sim \rho g \sin(\alpha) \sim \rho_{c_2} g d\tilde{h}/dx$ and $\rho_{c_2} g \cos(\beta) \sim \rho_{c_2} g (1-d\tilde{h}/dx)$. The equation of motion (Poiseuille/Couette flow) for a thin layer in the approximation of lubrication theory will be:

$$\begin{aligned} \frac{\partial \tau_{xy}}{\partial y} &= -\frac{\partial \tau_{yy}}{\partial x} \approx \frac{\partial p}{\partial x} - \rho_{c_2} g - \frac{\partial(\tilde{h}+w)}{\partial x} \\ \frac{\partial \tau_{yy}}{\partial y} &+ \frac{\partial \tau_{yx}}{\partial x} - \frac{\partial p}{\partial y} \approx -\rho_{c_2} g \left(1 - \frac{\partial(\tilde{h}+w)}{\partial x}\right) \\ \frac{\partial u_{c_2}}{\partial x} &+ \frac{\partial v_{c_2}}{\partial y} = 0 \end{aligned} \tag{B.4}$$

where pressure p is $p \approx P_0(x) + \bar{\rho}_c g(\tilde{y} + y_{13} + h)$; h is taken to be positive above sea-level; $\bar{\rho}_c$ is averaged crustal density.

In the simplest case of local isostasy, w and $\partial w/\partial x$ are approximately $\bar{\rho}_c/\Delta(\bar{\rho}_c - \rho_m) \sim 4$ times greater than $\tilde{h}$ and $d\tilde{h}/dx$, respectively. The pressure gradient due to Moho depression is $\rho_m g \partial(\tilde{h}+w)/\partial x$. "Correction" by the gradient of the gravitational potential energy density of crust yields $(\rho_m - \bar{\rho}_c) g \partial(\tilde{h}+w)/\partial x$ for the effective pressure gradient in the crust, with w being equal to $\tilde{h}((\rho_m - \bar{\rho}_c)/\rho_m)$. In the case of regional compensation, when the mantle lithosphere is strong, the difference between $\tilde{h}$ and w can be 2–3 times less. To obtain w, we solve the system of Eq. (A.1). Substitution of Eq. (B.3) to Eq. (B.4) gives:

$$\begin{aligned} \frac{\partial \tau_{xy}}{\partial y} &\approx \frac{\partial p}{\partial x} - \rho_{c_2} g \frac{\partial(\tilde{h}+w)}{\partial x} \\ \frac{\partial p}{\partial y} &\approx \rho_{c_2} g \left(1 - \frac{\partial(\tilde{h}+w)}{\partial x}\right) \\ \frac{\partial u}{\partial y} &= 2^n A^* (-H^*/RT) \left|\tau_{xy}\right|^{n-1} \tau_{xy} \\ \frac{\partial v}{\partial y} &= -\frac{\partial u}{\partial x} \end{aligned} \tag{B.5}$$

The value $1 - \partial(\tilde{h}+w)/\partial x \approx 1$ due to the assumption of small deflections ($w/T_e << L/T_e$, $\tilde{h} \sim 0.2$–$0.5w$, where L is the length of the plate). One has to note that strain rates of the lower crustal rocks (assuming quartz-controlled rheology) increase approximately by a factor of 2 for each ~20°C of temperature increase with depth [e.g., Bird, 1991]. This results in that the flow is being concentrated near the Moho, and the effective thickness of the transporting channel is much less than Δh_{c_2}.

Depth integration of Eq. (B.5) gives us the longitudinal and vertical components of the basic material velocity in the lower crust. For example, we have:

$$\begin{aligned} u &= \int_0^{h_{c2}-y_{13}} 2^n A^* \exp(-H^*/RT(\tilde{y})) \left|\tau_{xy}\right|^{n-1} \tau_{xy}\, \partial j \\ v\Big|_0^{h_{c2}-y_{13}} &= -\frac{\partial}{\partial x} \int_0^{h_{c2}-y_{13}} u \partial\tilde{y} \approx \frac{\partial(\tilde{h}+w)}{\partial t} \end{aligned} \tag{B.6}$$

The later equation gives the variation of thickness of the ductile channel in time (equal to the difference between the vertical flow at the top and bottom boundaries). Lobkovsky (1988) (see also Lobkovsky and Kerchman, 1991), Bird (1991) already gave an analytical solution for evolution of the topography dh/dt due to ductile flow in the crustal channel for the case of local isostatic equilibrium (zero strength of the upper crust and mantle). Kaufman and Royden (1994) provide a solution for the case of elastic mantle lithosphere but for Newtonian rheology. In our case, the irregular time-dependent load is applied on the surface, and nonlinear rheology is assumed both for the ductile and competent parts of the lithosphere. Hence, no analytical solution for u and v can be found and we choose to obtain u and v through numerical integration.

The temperature which primarily controls the effective viscosity of the crust, is much lower in the uppermost and middle portions of the upper crust (first 10–15 km in depth). As a result, the effective viscosity of the middle portions of the upper crust is 2–4 orders higher than that of the lower crust (10^{22} to 10^{23} Pa s compared to 10^{18} to 10^{20} Pa s, Eqs. (7, 8)). Therefore, we can consider the reaction of the lower crust to deformation of the upper crust as rapid. The uppermost parts of the upper crust are brittle (Figs. 2 and 5), but in calculation of the flow they can be replaced by some depth-averaged viscosity defined as $\bar{\mu}_{eff} = \bar{\sigma}^d/2\dot{\varepsilon}$ (Beekman, 1994). In spite of some negligence by the underlying principles, this operation does not introduce significant uncertainties to the solution because the thickness of the "brittle" crust is only 1/4 of the thickness of the competent crust. Analogously to the ductile (mostly lower) crust, we can extend the solution of the equations for the horizontal f low to the stronger upper portions of the upper crust. However, due to high-

er viscosity, and much lower thickness of the strong upper crustal layers, one can simply neglect the perturbations of the flow velocity there and assume that $v = v(y \le y_{13})$, $u = u(y \le y_{13})$ (y is downward positive). For numerical reasons, we cut the interval of variation of the effective viscosity at 10^{19} to 10^{24} Pa s.

Solution for the channel flow implies that the channel is infinite in both directions. In our case the channel is semi-infinite, because of the condition $u = 0$ at $x = 0$ beneath the axis of the mount. Thin flow approximation thus cannot be satisfied beneath the mount because of the possibility of a sharp change of its thickness. Therefore, we need to modify the solution in the vicinity of $x = 0$. This could be done using a solution for the ascending flow for $x < a_l$. An analytical formulation for the symmetric flow in the crust and definition for the critical distance a_l are given in Appendix C. There we also explain how we combine the solution for the ascending symmetric flow beneath the axis of the mountain range with the asymptotic solution for Poiseuille/Couette flow for domains off the axis. A similar approach can be found in literature dealing with cavity-driven problems (e.g., Hansen and Kelmanson, 1994). However, most authors (Lobkovsky and Kerchman, 1991; Bird and Gratz, 1990) ignore the condition $u = 0$ at $x = 0$ and the possibility of large thickness variations and simply considered a thin infinite channel.

Boundary Conditions

We have chosen simplest boundary conditions corresponding to the flow approximations. Thus, the velocity boundary conditions are assumed on the upper and bottom interfaces of the lower crustal channel. Free flow is the lateral boundary condition. The velocity condition also could be combined with a pre-defined lateral pressure gradient.

A link between the competent parts of the lithosphere and flow in the ductile parts is effectuated through the conditions of continuity of stress and velocity.

The problem of choice of boundary conditions for continental problems has no unique treatment. Most authors apply vertically homogeneous stress, force or velocity on the left and right sides of the model plate, Winkler-type restoring forces as bottom vertical condition, and free surface/normal stress as a upper boundary condition (e.g., England and McKenzie, 1983; Chery et al., 1991; Kusznir, 1991). Other authors use shear traction (velocity/stress) at the bottom of the mantle lithosphere (e.g. Ellis et al., 1995). Even choice between stress and force boundary conditions leads to significantly different results. Yet, the only observation that may provide an idea on the boundary conditions in nature comes from geodetic measurements and kinematic evaluations of surface strain rates and velocities. The presence of a weak lower crust leads to the possibility of differential velocity, strain partitioning between crust and mantle lithosphere and to possibility of loss of the material from the system due to outflow of the ductile crustal material (e.g. Lobkovsky and Kertchman, 1991; Ellis et al., 1995). Thus the relation between the velocities and strain rates observed at the surface with those on the depth is unclear. It is difficult to give preference to any of the mentioned scenarios. We have thus chosen the simplest one.

Appendix C
Analytical Formulation for Ascending Crustal Flow

In the general case of non-inertial flow (low Reynolds number), a symmetric flow problem (flow ascending beneath the mount) can be resolved from the solution of the system of classical viscous flow equations (Fletcher, 1988; Hamilton et al., 1995):

$$\begin{aligned} 0 &= \rho_{c2} F_x - \frac{dp}{dx} + \frac{\partial}{\partial y}\left(2\mu\left(\frac{\partial u}{\partial y} + \frac{\partial v}{\partial x}\right)\right) \\ 0 &= \rho_{c2} F_y - \frac{dp}{dy} + \frac{\partial}{\partial x}\left(2\mu\left(\frac{\partial u}{\partial y} + \frac{\partial v}{\partial x}\right)\right) \\ \frac{\partial u}{\partial x} &+ \frac{\partial v}{\partial y} = 0 \end{aligned} \qquad \text{(C.1)}$$

We define $\partial p/\partial x \approx \partial \tilde{p}/\partial x + g(\rho_{c_2}\partial w/\partial x + \rho_{c_1}\partial(du)/\partial x)$, $du \approx d\tilde{h}$ and $\partial p/\partial y = \partial \tilde{p}/\partial y - g\rho_{c_2}$where $\tilde{p}$ is dynamic, or modified pressure. The flow is naturally assumed to be Couette/Poiselle flow away from the symmetry axis (at a distance a_l). a_l is equal to 1–2 thicknesses of the channel, depending on channel thickness-to-length ratio. In practice a_l is equal to the distance at which the equivalent elastic thickness of the crust (T_{ec}) becomes less than ~5 km due to flexural weakening by elevated topography. For this case, we can neglect the elasticity of the upper surface of the crust and use the condition of the stress-free upper surface. The remote feeding flux q at $x \to \pm a_l$ is equal to the value of flux obtained from depth integration of the channel source (Couette flow), and free flow is assumed as a lateral boundary condition. The flux q is determined as $q \sim \int u dy$ (per unit length in z direction). This flux feeds the growth of the topography and deeping of the crustal root. Combination of two flow formulations is completed using the depth integrated version of the continuity equation and global continuity equation [Huppert, 1982] :

$$\int \frac{\partial v}{\partial y}\,dy + \frac{\partial}{\partial x}\left(\int u dy\right) = 0 = \frac{\partial(\tilde{h}+w)}{\partial t} + \frac{\partial q}{\partial x}$$
$$q\big|_{x=a_l,\,x\le a_l} = q\big|_{x=a_l,\,x\ge a_l}$$
$$\underbrace{\int_{o}^{a_l(\phi)}(\tilde{h}+w)\,dx}_{\text{ascending flow}} + \underbrace{\int_{a_l(\phi)}^{\infty}(\tilde{h}+w)\,dx}_{\text{channel flow}} = qt^{\theta}, \qquad \text{(C.2)}$$

where θ is some non-negative constant, $\theta = 1$ in our case. With that we can combine solutions for horizontal flow far off the mount axis (Couette/Poiseuille flow) with solutions for ascending flow below the mount (e.g., Hansen and Kelmanson, 1994). Assuming a new local coordinate system $x' = x$, $y' = -y-(h_{c_2}+(h_{c_2}-y_{13})/2)$, the boundary conditions for the flow ascending near the symmetry axis would be $u = v = 0$; $du/dy' = 0$ at $x' = 0$, $y' = 0$ (beneath the mount axis). Then, we assume that the viscosity (μ) in the ascending flow is constant and equal to $\bar{\mu} = \bar{\mu}(a_l)$ where $\bar{\mu}(a_l)$ is the depth-averaged value of the effective non-linear viscosity defined from the solution for the channel flow (Appendix B) at distance $x = a_l$. Use of constant viscosity is, however, not a serious simplification for the problem as a whole, because a_l is small and thus this simplification applies only to a small fraction of the problem.

Introducing the vorticity function $\xi = \mathrm{rot}\,\mathbf{v} = \partial u/\partial y - \partial v/\partial x = \nabla^2\psi$, assuming laminar flow, we then write Stoke's equations as (Talbot and Jarvis, 1984; Fletcher, 1988; Hamilton et al., 1995):

$$\mu\frac{\partial \xi}{\partial x} = \frac{\partial p}{\partial y}$$
$$\mu\frac{\partial \xi}{\partial y} = -\frac{\partial p}{\partial x} \qquad \text{(C.3)}$$
$$\xi = \nabla^2\psi$$

At the upper surface of the fluid, streamline $\psi = 0$, is taken to be stress-free (low T_{ec}, see above) which leads to the following conditions: $p\cos 2\alpha = 2\mu\partial^2\psi/\partial y'\partial x$; $p\sin 2\alpha = \mu(\partial^2\psi/\partial x^2 - \partial^2\psi/\partial y'^2)$. Here α is downward inclination of the surface to the horizontal. Finally, the symmetry of the flow requires $\psi(-x,y') = -\psi(x,y')$.

The general solution in dimensionless variables (Talbot and Jarvis, 1984): $X = h_{max}x'$; $Y = h(0)y'$; $p = (\mu q/\pi h_{max}^2)p'$; $\psi = (q/\pi)\psi'$, where h_{max} is the maximum height of the free surface, is:

$$\psi = \tan^{-1} X/Y + XY/(X^2+Y^2) +$$
$$+\sum_{n=0}^{\infty}(-1)^n(n+1)Y^{2n+2}((2n+2)!)^{-1}f^{(2n)}(X) +$$
$$+\sum_{n=0}^{\infty}(-1)^n(n+1)Y^{2n+3}((2n+3)!)^{-1}\gamma^{(2n)}(X);$$

$$p = K - \lambda Y + 2(Y^2-X^2)/(X^2+Y^2)^2 + \qquad \text{(C.4)}$$
$$+\sum_{n=0}^{\infty}(-1)^n X^{2n+1}((2n+1)!)^{-1}f^{(2n+1)}(X) - G(X) +$$
$$+\sum_{n=0}^{\infty}(-1)^n Y^{2n+2}((2n+2)!)^{-1}\gamma^{(2n+1)}(X)$$
$$G(X) = \int_0^X \gamma(s)\,ds$$

f and γ are arbitrary functions of expansion series and $f^{(j)}$, $\gamma^{(j)}$ are their j^{th} derivatives, $\lambda = \pi\rho g h_{max}^3/\mu q$, K is constant. γ and f are determined numerically because the expressions for ψ and p are nonlinear and cannot be solved analytically. The calculation of ψ and p is done on the assumption of small curvature of the free surface which allows linear approximation of γ and f, i.e., as $\gamma = AX$ and $f = BX$. Then the free surface can be searched in the form of a parabolic function , e.g., $\tilde{h} \sim C - DX^2$ (Talbot and Jarvis, 1984).

The assumptions of constant viscosity and stress-free upper surface are questionable. To avoid this problem, we can solve Eqs. (B.1) for the ascending flow analogously to how it was done for the channel flow (Appendix B). The solution to Eq. (B.1) in the case of the ascending flow can be obtained assuming $\mu = \mu(y)$, $\tau_{xy}(x,0) \neq 0$ and $U = u$ and $V = \Phi(y)$ where $\Phi(y)$ is to be determined. Here we simplify Eq. (B.1c) by assuming that the viscosity is only depth dependent, which is a better approximation to the nonlinear law (8) than the assumption of constant viscosity.

The primary boundary conditions are $U(0,y) = 0$ (symmetric flow), $\tau_{xy}(x,y^*) = 0$ (assumption of the existence of a shear-free surface at some depth y^*, e.g., depth of compensation), $\tau_{xy}(x,0) = \tau_e$, $p(x,0) = \bar{\rho}_c g(h+y_{13})$ (shear stress and pressure continuity on the boundary with the overlying competent upper crustal layer of effective thickness y_{13}).

From $U(0,y) = 0$, (B.1a), $v = \Phi(y)$, we get:

$$U = x\partial\Phi(y)/\partial y;$$
$$\sigma_{xx,yy} = \pm 2\mu\partial\Phi(y)/\partial y;\ \tau_{xy} = x\mu\partial^2\Phi(y)/\partial y^2. \qquad \text{(C.5)}$$

With the assumption that $y^* \ll a_l$ and from (B.1a) this yields:

$$\partial^2\tau_{xy}/\partial x^2 - \partial^2\tau_{xy}/\partial y^2 + 2\partial^2\sigma_{xx}/\partial x\partial y -$$
$$-\partial Fx/\partial y + \partial Fy/\partial x = 0 \qquad \text{(C.6)}$$

which provides the expression for $\Phi(y)$ ($\partial F_x/\partial y$ and $\partial F_y/\partial x \approx 0$):

$$\partial^2(\mu\partial^2\Phi(y)/\partial y^2)\partial y^2 = 0, \text{ or } \partial^2\tau_{yy}/\partial y^2 = 0 \qquad (C.7)$$

With the conditions $\tau_{xy}(x,y^*) = 0$, $\tau_{xy}(x,0) = \tau_e$ and under assumption that $\partial y^*/\partial x$ is small, we can obtain: $\tau_{xy}(x,y) \approx \tau_e(1-y/y^*)$ and $p(x,y) \approx x^2\partial(\mu\partial^2\Phi(y)/\partial y^2)\partial y + C_1(y)$. $C_1(y)$ is to be found from the boundary conditions on p (Davies, 1994).

Since the expressions for stress are defined, the velocities U and V can be obtained from integration of Eqs. (B.1a,b) relating stress components and du/y, dv/y. We have to determine the constants of integration in a way providing continuity with the solution for the channel flow at $x = a_l$. For that we define the boundary conditions at $x = \pm a_l$: $U(\pm a_l,y) = u_l$; $V(\pm a_l, y) = v_l(\pm a_l, y)$ (where u_l and v_l are provided by the solution for channel flow).

As pointed out by Davies (1994), it is impossible to provide an analytical or simplified semi-analytical solution for the case when the viscosity μ is defined exactly through the power law (8).

Appendix D
Numerical Algorithm for the Full Thermo-Mechanical Model

This mixed finite-element volume/finite difference code Parovoz is based on the FLAC technique (Cundall, 1989). It solves simultaneously Newtonian dynamic equations of motion (A1), in a Lagrangian formulation, coupled with visco-elasto-plastic constitutive equations (A2), heat transport equations (A3), and state equation (A4) (see Appendix A, (Burov et al., 2001; Le Pourhiet et al., 2004) for details concerning numerical implementation).

$$\left\langle \rho \frac{\partial \mathbf{v}}{\partial t} \right\rangle - div\boldsymbol{\sigma} - \rho\mathbf{g} = 0 \qquad (D1)$$

$$\frac{D\sigma}{Dt} = F(\sigma, \varepsilon, \mathbf{v}, \nabla\mathbf{v}, \ldots T \ldots) \qquad (D2)$$

$$\rho C_p\partial T/\partial t + \mathbf{v}\nabla T - k_c div(\nabla T) - H_r - \\ - frac\times\sigma_{II}\partial\varepsilon_{II}/\partial t = 0 \qquad (D3)$$

assuming adiabatic temperature dependency for density and Boussinesq approximation for thermal body forces:

$$\rho = \rho_0 (1 - \alpha\Delta T) \qquad (D4)$$

Here $\mathbf{v}$, $\boldsymbol{\sigma}$, $\mathbf{g}$, k_c are the respective terms for velocity, stress, acceleration due to body forces, and thermal conductivity. The brackets in Eq. (A1) specify conditional use of the related term: in quasi-static mode, the inertia is dumped using inertial mass scaling (Cundall, 1989). The terms t, ρ, C_p, T, H_r, α, $frac\times\sigma_{II}\partial\varepsilon_{II}/\partial t$ designate respectively time, density, specific heat, temperature, internal heat production, thermal expansion coefficient, and shear heating term moderated by experimentally defined *frac* multiplier (*frac* was set to 0 in our experiments). The terms $\partial/\partial t$, $D\sigma/Dt$, F are a time derivative, an objective (Jaumann) stress time derivative, and a functional, respectively. In the Lagrangian framework, the incremental displacements are added to the grid coordinates allowing the mesh to move and deform with the material. This enables solution of large-strain problems locally using small-strain formulation: on each time step the solution is obtained in local coordinates, which are then updated in the large strain mode. Volume / density changes due to phase transitions are accounted via application of equivalent stresses to affected material elements.

Solution of Eq. (A1) provides velocities at mesh points used for computation of element strains and of heat advection $\mathbf{v}\nabla T$. These strains are used in Eq. (A2) to calculate element stresses, and the equivalent forces are used to compute velocities for the next time step.

All rheological terms are implemented explicitly. The rheology model is serial viscous-elastic-plastic (Table 1). The plastic term is given by explicit Mohr-Coulomb plasticity (non-associative with zero dilatency) assuming a linear Navier-Coulomb criterion. We imply internal friction angle ϕ of 30° and maximal cohesion S of 20 Mpa, which fit best the experimental Byerlee's law of rock failure (Byerlee, 1978):

$$\tau = S + \sigma_n \operatorname{tg}\phi \qquad (D5)$$

where τ is the shear stress and σ_n is the normal stress. Linear cohesion softening is used for better localization of plastic deformation ε_p ($S(\varepsilon_p) = S_0$ min (0, $1-\varepsilon_p/\varepsilon_{p_0}$) where ε_{p_0} is 0.01).

The ductile-viscous term is represented by nonlinear power law with three sets of material parameters (Table 1) that correspond to the properties of four lithological layers: upper crust (quartz), middle-lower crust (quartz-diorite), mantle, and asthenosphere (olivine):

$$\mu_{\text{eff}} = \left(\frac{\partial\varepsilon}{\partial t}\right)_{II}^{d(1-n)/n} (A^*)^{-1/n} \exp(H/nRT) \qquad (D6)$$

where $\left(\frac{\partial\varepsilon}{\partial t}\right)_{II}^{d} = \left(Inv_{II}\left(\frac{\partial\varepsilon_{ij}}{\partial t}\right)\right)^{1/2}$

is the effective strain rate and $A^* = \frac{1}{2}A\cdot 3^{(n+1)/2}$ is the material constant, H is the activation enthalpy, R is the

gas constant, n is the power law exponent (Table 1b). The elastic parameters (Table 1a) correspond to commonly inferred values from Turcotte and Schubert (1982).

Surface processes are taken into account by diffusing (D7) the topographic elevation h of the free surface along x using conventional Culling erosion model (Culling, 1960) with a diffusion coefficient k.

$$\frac{\partial^2 h}{\partial t^2} = k \frac{\partial^2 h}{\partial x^2} \tag{D7}$$

This simple model is well suited to simulate fan deltas, which can be taken as a reasonably good analogue of typical foreland basin deposits. This model is not well adapted to model slope-dependent long-range sedimentation, yet, it accounts for some most important properties of surface processes such as dependency of the erosion/sedimentation rate on the roughness of the relief (surface curvature).

PARA(O)VOZ allows for large displacements and strains in particular owing to an automatic remeshing procedure, which is implemented each time the mesh becomes too destorted to produce accurate results. The remeshing criterion is imposed by a critical angle of grid elements. This angle is set to 10° to reduce frequency of remeshing and thus limit the associated numerical diffusion. The numerical diffusion was effectively constrained by implementation of the passive marker algorithm. This algorithm traces passively moving particles that are evenly distributed in the initial grid. This allows for accurate recovering of stress, phase, and other parameter fields after each remeshing. PARA(O)VOZ has been already tested on a number of geodynamical problems for subduction/collision context (Burov et al., 2001; Toussaint et al., 2004a, 2004b).